

A painless multi-level automatic goal-oriented hp -adaptive coarsening strategy for elliptic and non-elliptic problems[☆]

Felipe V. Caro^{a,b,*}, Vincent Darrigrand^d, Julen Alvarez-Aramberri^b, Elisabete Alberdi^b,
David Pardo^{b,a,c}

^a Basque Center for Applied Mathematics (BCAM), Bilbao, Spain

^b University of the Basque Country (UPV-EHU), Leioa, Spain

^c Ikerbasque, Bilbao, Spain

^d CNRS-IRIT, Toulouse, France

Received 2 May 2022; received in revised form 30 August 2022; accepted 4 September 2022

Available online 6 October 2022

Abstract

This work extends an automatic energy-norm hp -adaptive strategy based on performing quasi-optimal unrefinements to the case of non-elliptic problems and goal-oriented adaptivity. The proposed approach employs a multi-level hierarchical data structure and alternates global h - and p -refinements with a coarsening step. Thus, at each unrefinement step, we eliminate the basis functions with the lowest contributions to the solution. When solving elliptic problems using energy-norm adaptivity, the removed basis functions are those with the lowest contributions to the energy of the solution. For non-elliptic problems or goal-oriented adaptivity, we propose an upper bound of the error representation expressed in terms of an inner product of the specific equation, leading to error indicators that deliver quasi-optimal hp -unrefinements. This unrefinement strategy removes unneeded unknowns possibly introduced during the pre-asymptotical regime. In addition, the grids over which we perform the unrefinements are arbitrary, and thus, we can limit their size and associated computational costs. We numerically analyze our algorithm for energy-norm and goal-oriented adaptivity. In particular, we solve two-dimensional (2D) Poisson, Helmholtz, convection-dominated equations, and a three-dimensional (3D) Helmholtz-like problem. In all cases, we observe exponential convergence rates. Our algorithm is robust and straightforward to implement; therefore, it can be easily adapted for industrial applications.

© 2022 Elsevier B.V. All rights reserved.

Keywords: Goal-oriented adaptivity; hp -adaptivity; Finite element method; Unrefinements; Non-elliptic problems

[☆] David Pardo has received funding from: the European Union's Horizon 2020 research and innovation program under the Marie Skłodowska-Curie grant agreement No. 777778 (MATHROCKS); the European Regional Development Fund (ERDF) through the Interreg V-A Spain-France-Andorra program POCTEFA 2014–2020 Project PIXIL (EFA362/19); the Spanish Ministry of Science and Innovation projects with references PID2019-108111RB-I00 (FEDER/AEI) and PDC2021-121093-I00 (AEI/Next Generation EU), the “BCAM Severo Ochoa” accreditation of excellence (SEV-2017-0718); and the Basque Government through the BERC 2022-2025 program, the three Elkartek projects 3KIA (KK-2020/00049), EXPERTIA (KK-2021/00048), and SIGZE (KK-2021/00095), and the Consolidated Research Group MATHMODE (IT1294-19) given by the Department of Education. Vincent Darrigrand is supported by the EU under the Horizon 2020 Project Energy oriented Center of Excellence: toward exascale for energy (EoCoE-II), Project ID: 824158. Julen Alvarez-Aramberri is supported by the European Union-Next GenerationEU.

We thank Luis E. García-Castillo for his technical advice and his insightful comments.

* Corresponding author at: Basque Center for Applied Mathematics (BCAM), Bilbao, Spain.

E-mail addresses: fcaro001@ikasle.ehu.eus (F.V. Caro), vincent.darrigrand@gmail.com (V. Darrigrand), julen.alvarez@ehu.eus (J. Alvarez-Aramberri), elisabete.alberdi@ehu.eus (E. Alberdi), dzubiaur@gmail.com (D. Pardo).

<https://doi.org/10.1016/j.cma.2022.115641>

0045-7825/© 2022 Elsevier B.V. All rights reserved.

1. Introduction

The Finite Element Method (FEM) is commonly employed to approximate solutions of Partial Differential Equations (PDEs) that govern multiple physical phenomena. This numerical technique allows to handle complex geometries (see, e.g., [1,2] among others) and model a wide variety of physical problems and engineering applications. However, the computational cost required to obtain accurate finite element solutions often becomes prohibitive, and it is then necessary to develop specific strategies to minimize the solution cost.

The design of efficient meshes is one of the available tools to minimize computational costs. There exist multiple adaptive FEMs to perform this task. For example, h -adaptive FEMs [3] reduce the mesh size h locally while keeping fixed the polynomial order of approximation p . p -adaptive FEMs [4] enrich locally the polynomial space p while the mesh size h remains invariant. The combination of both approaches leads to the so-called hp -adaptive FEM [5].

We encounter different hp -adaptive algorithms in the literature. For example, the so-called Texas three-step strategy [6] alternates between h - and p -refinements but leads to non-optimal results. The work of Demkowicz et al. [7–9] produces optimal meshes by minimizing a local projection error based on a reference solution. This approach, widely utilized in diverse applications [10–16], requires a Projection-Based Interpolation (PBI), which might be complex to implement. Furthermore, it calculates the reference solution over a globally refined $(\frac{h}{2}, p+1)$ -grid, which is often prohibitively expensive to compute. The authors of [17] proposed a hp -strategy based on the local regularity of the exact solution. Nonetheless, its wide industrial applications are unclear, a problem that this approach typically shares with some Discontinuous Galerkin (DG) methods [18,19]. For a further review and comparison among some of the existing hp -adaptive strategies (up to 2014), we refer the reader to [20].

The implementation of high-order hp -meshes is challenging. Specifically, when performing local h -refinements, *hanging nodes* appear naturally (see, e.g., [8,21]), and to guarantee the continuity of the solution, we need to constrain them. The data structures needed to deal with hanging nodes are rather complicated and have numerous technical difficulties. To avoid these inconveniences and limit the implementation complexity, Zander et al. [22] proposed a suitable data structure that supported hp -discretizations while eliminating the hanging nodes by construction. This approach employs hierarchical basis functions in h and p in a multi-level grid, and performs uniform refinements with massive use of Dirichlet nodes to ensure continuity and enable local refinements. It is also possible to replace global uniform refinements by isotropic refinements over a subset of elements. This vast utilization of Dirichlet nodes avoids introducing hanging nodes and highly simplifies the existing data structures to handle hp -refinements. Kopp et al. extended these data structures to arbitrary dimensions [23] and space–time discretizations [24].

In 2020, Darrigrand et al. [25] introduced a novel automatic hp -adaptive mesh-refinement strategy for elliptic problems based on Zander’s data structures [22,26,27]. In addition to bypassing the mesh irregularities caused by hanging nodes, the main achievement was to avoid complex implementations such as local projections (see, e.g., PIB [7]) that require simultaneously maintaining multiple grids in the data structures. This easy-to-implement hp -strategy performs a general (user-defined) refinement step followed by a specific coarsening of the mesh. In particular, we employ quadrilateral elements and alternate global h - or p -refinements with local and quasi-optimal hp -unrefinements (similarly to [28,29]). For that purpose, we eliminate the basis functions with the lowest contributions to the energy of the solution at each hp -unrefinement step. We notice that, although it would be possible to construct suitable a posteriori error estimators [30] to enhance the refinement step of the algorithm, this possibility is out of the scope of this work.

While most existing approaches execute optimal hp -refinement steps, the aforementioned coarsening-based strategy provides a particular advantage: it is capable of *correcting* some previous *mistakes* by removing undesired basis functions, possibly introduced via global refinements or during the pre-asymptotic regime. Moreover, later unrefinement iterations can also correct possible non-optimal results due to the assumed quasi-orthogonality approximation of the basis functions.

Instead of controlling the energy of the solution over the entire domain, many engineering applications aim to control errors in a specific quantity of engineering interest, and often only in certain parts of the domain. This fact motivated the development of the so-called Goal-Oriented Adaptive (GOA) strategies [31–34] as an attempt to build mesh adaptation procedures designed to approximate particular Quantities of Interest (QoI) with a reduced computational cost. GOA algorithms are standard in many engineering applications. For instance in electromagnetics [35–38], structural problems and visco-elasticity [39–41], fluid–structure interactions [42–45], or control theory [46–48]. In particular, GOA hp -adaptive algorithms deliver exponential convergence rates in terms

of a specific property of the solution (see, e.g., [49–53] for numerical results) even though convergence proofs are not customary [54].

Darrigrand’s energy-based-adaptive hp -strategy [25] is restricted to elliptic problems. Thus, the main contributions of this work are to extend this method to (a) non-elliptic equations and (b) GOA approaches for elliptic and non-elliptic problems. For energy-based adaptive strategies applied to non-elliptic equations, we provide an alternative estimation of the energy contribution in terms of an inner product depending upon the bilinear form of the problem. For the GOA approach, we use the adjoint problem to construct an upper bound of the error representation expressed in terms of an inner product that depends on the bilinear form of the problem. As a result, we obtain an automatic goal-oriented hp -adaptive algorithm for elliptic and non-elliptic problems.

Remarkably, our algorithm is robust and straightforward to implement, and therefore, it might be of interest to industrial applications. Besides, our approach avoids the computation of reference solutions on very fine grids, as in other methods like [7]. We restrict ourselves to anisotropic p and isotropic h -refinements, and we highlight a recent work by Zander et al. [55] to extend the multi-level data structures to support anisotropic h -refinements. We test and analyze our algorithm in three different 2D problems based on Poisson, Helmholtz, and convection-dominated equations, and we also provide numerical results for a 3D Helmholtz-like problem.

We organize the remainder of this work as follows: Section 2 describes the data structures and introduces the concept of *removable* basis functions, a crucial idea in our approach. In Section 3, we define the adaptive strategy and provide element-wise error indicators that guide the adaptivity for energy-norm and goal-oriented adaptivity applied to elliptic and non-elliptic problems. Section 4 illustrates the performance of our method numerically. In particular, we show the exponential convergence behavior of the approach for a wide range of 2D and 3D problems, and we exhibit different final h - and hp -adapted meshes. Finally, we present our conclusions in Section 5.

2. Data structures

Classical adaptive schemes often refine a starting coarse mesh to obtain finer ones. While performing local h - or hp -refinements, *hanging nodes* appear, and they should be constrained to guarantee the global continuity of the approximate solution. This fact often poses serious implementation difficulties (see, e.g., [56]).

In 1971, Mote [57] proposed an alternative procedure based on the idea of refining by superposition. This approach, nowadays known as superposition techniques, maintains an initial *base* discretization unmodified and subsequently overlaps one (or several) finer *overlay* mesh(es). Accordingly, the initial coarse grid captures the large-scale characteristics of the solution while the overlaying mesh(es) reproduces the small-scale features. In 2015, Zander et al. [22] took advantage of this superposition idea and proposed a data structure that enables local hp -mesh refinements and unrefinements while easily handling the constrained *hanging nodes* that naturally appear during local h -refinements (see, e.g., [8,21]).

Following the data structures introduced in [22], we impose a massive number of Dirichlet nodes throughout the overlay mesh(es), thus ensuring the continuity of the solution by construction. Basically, in the overlay meshes, we only add globally continuous *basis functions* (see Fig. 1) rather than possibly discontinuous *shape functions* (see [22,25]). That leads to a rather simple implementation where imposing the one-irregularity rule [7] is unnecessary. In addition, to guarantee the linear independence of the basis functions, high-order basis functions are only activated on those elements with no further refinements in h (see Fig. 1). Such elements without further refinements may be encountered even in the initial level of the mesh in the case of unrefined elements. In particular, when performing an h -refinement, high-order basis functions are transferred to the children. For further details, we refer the reader to [27].

2.1. Removable basis functions in a multi-level hp -mesh

In 2020, Darrigrand et al. [25] proposed an easy-to-implement hp -adaptive strategy for elliptic problems that exploited Zander’s data structures [27]. The main idea of this work consists of incorporating a coarsening strategy that identifies the basis functions that can be *directly* removed. Hence, we define these *removable* basis functions as those we can eliminate from the discretization without modifying any other basis function and preserving complete polynomial spaces. Fig. 1 shows the removable basis functions in red and non-removable basis functions in black.

For 2D and 3D problems, our current implementation defines the basis functions as tensorial products of the 1D basis functions. Additionally, we incorporate anisotropic p and isotropic h refinements. However, according to the

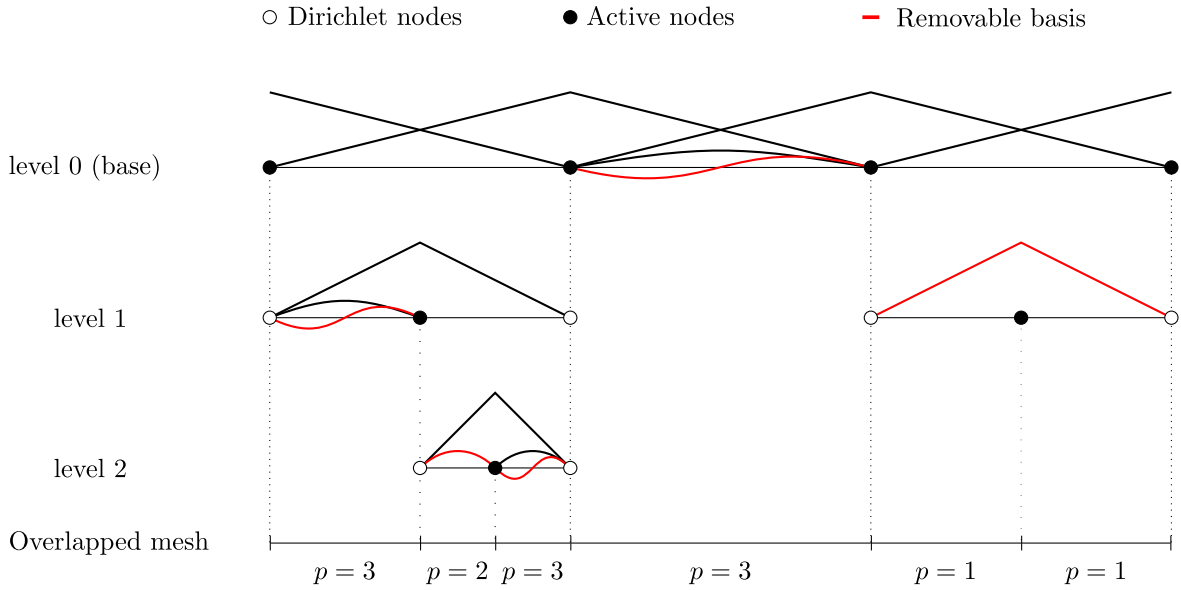


Fig. 1. Illustration of a 1D multi-level hp -grid with hierarchical basis functions and Dirichlet nodes. *Removable* basis functions are indicated in red.

recent work of Zander et al. [55], it could be possible to extend these ideas to anisotropic h -refinements. To find specific details about the discretization and the properties of the genealogy tree (which are beyond the scope of this article), we refer to [25], and for further details and the specifications about the extension to 2D and 3D data structures, we refer to [27].

3. Adaptivity

This section describes our adaptive strategy, and we provide the error indicators that guide the hp -unrefinement steps. We start by algorithmically explaining our mesh generation and coarsening policy. After that, we introduce the concept of *projectors* in the context of a single finite element mesh, which allows us to simulate the presence of a second grid while only operating with one. Finally, we derive the error indicators employed in the coarsening steps for energy-norm and goal-oriented strategies and elliptic and non-elliptic problems.

3.1. Unrefinement policy

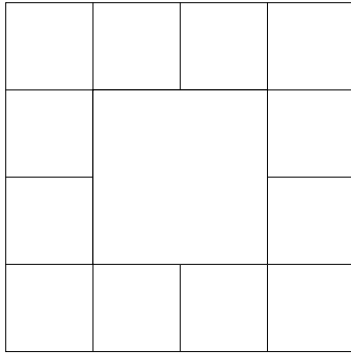
Adaptive FEMs aim to reduce computational costs while providing low discretization errors. In this work, we employ the adaptive algorithm introduced in [25], which iterates along with the following two steps for a given hp -grid:

1. To perform a user-defined mesh refinement (in our particular implementation, we alternate global and uniform h - and $p = p + 2$ -refinements), and then
2. To perform a (quasi)-optimal hp -coarsening step.

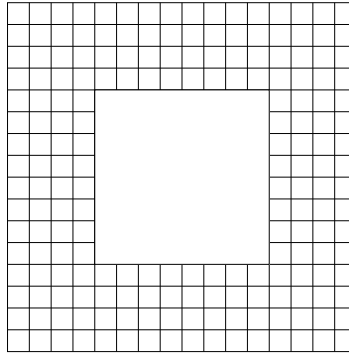
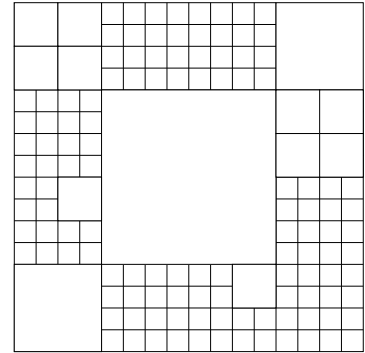
This procedure is illustrated in Algorithm 1. We emphasize that these repeated uniform global refinements guarantee the convergence of the approach, while the coarsening step ensures the almost optimal convergence rates [28,29].

Similarly to [25], the main ingredients of our hp -coarsening step (see Algorithm 2) are:

1. To compute the solution on the current mesh.
2. For each element of the mesh:
 - (a) To find the removable basis functions whose support contains the element.
 - (b) To calculate the contribution of the removable basis functions to the solution.

Algorithm 1: Adaptive process**Input:** A given initial mesh**Output:** A final hp -adapted mesh**while** $error > tolerance$ **do** Perform a global and uniform (h or p) refinement; Execute a (quasi)-optimal hp -coarsening step (Algorithm 2) to the mesh; Update $error$;**end**

(a) A initial (given) mesh.

(b) An h -refined mesh.(c) An h -adapted mesh.**Fig. 2.** Adaptive process illustrated.

3. Remove the basis functions with small contributions.

The above process is repeated until no basis function is eliminated. Fig. 2 illustrates the h -unrefinement policy. A given coarse mesh in Fig. 2(a) is h -refined globally in Fig. 2(b). Then, after an unrefinement process, we obtain the adapted mesh displayed in Fig. 2(c).

The definition of the contributions of the removable basis functions to the solution is problem-dependent. To provide representative quantities for energy-norm-based and GOA strategies over elliptic and non-elliptic problems, we first introduce our *projectors* in the context of a single finite element grid.

Algorithm 2: hp -unrefinement policy**Input:** A given mesh**Output:** An hp -unrefined mesh**do**

Compute the solution on the current mesh;

Compute the element-wise error indicators;

Unrefine the mesh by eliminating the removable basis functions with low error indicators;

When no contributions are below a given tolerance, exit;

end ;

3.2. Projectors

For dimension $d \in \{1, 2, 3\}$, let $\Omega \subset \mathbb{R}^d$ be an open bounded domain with a Lipschitz-continuous boundary $\partial\Omega$, and let $\mathbb{H}(\Omega)$ be a Hilbert functional space on Ω (simply denoted as \mathbb{H} in the following). For a given bilinear continuous form b defined on $\mathbb{H} \times \mathbb{H}$, let us define our problem with the following abstract variational formulation:

$$\begin{array}{|l} \text{Find } u \in \mathbb{H} \text{ such that} \\ b(u, \phi) = f(\phi), \quad \forall \phi \in \mathbb{H}, \end{array} \quad (1)$$

where f is a linear form. The discrete counterpart of this abstract variational formulation reads as follows:

$$\begin{array}{|l} \text{Find } u_{\mathcal{F}} \in \mathbb{H}_{\mathcal{F}} \text{ such that} \\ b(u_{\mathcal{F}}, \phi_{\mathcal{F}}) = f(\phi_{\mathcal{F}}), \quad \forall \phi_{\mathcal{F}} \in \mathbb{H}_{\mathcal{F}}, \end{array} \quad (2)$$

where $\mathbb{H}_{\mathcal{F}} := \text{span}\{\phi_1, \dots, \phi_{n_{\mathcal{F}}}\}$ is a finite element discretization \mathcal{T} of \mathbb{H} , such that $\mathbb{H}_{\mathcal{F}} \subset \mathbb{H}$, $\mathcal{F} = \{\phi_i\}_{i=1}^{n_{\mathcal{F}}}$ is a set of basis functions ϕ_i , and $n_{\mathcal{F}} = \dim(\mathbb{H}_{\mathcal{F}})$. Besides, $u_{\mathcal{F}}$ corresponds to the Galerkin approximation of u in $\mathbb{H}_{\mathcal{F}}$.

Some *hp* techniques handle a fine and coarse mesh at the same time (see, e.g., [8,9]). In addition to the coding difficulties derived from this fact, they typically need to define and implement rather complex projection operators (such as the PBI) to link both grids. One of the main characteristics of our “painless” approach is to operate always on a single mesh. While it simplifies the implementation, it requires defining a projector that simulates the presence of a coarse mesh without the trouble of handling one.

For a given subset of basis functions $\mathcal{S} \subset \mathcal{F}$ that generates the space $\mathbb{H}_{\mathcal{S}} \subset \mathbb{H}_{\mathcal{F}}$, we define our *projection operator* $\Pi_{\mathcal{F}}^{\mathcal{S}}: \mathbb{H}_{\mathcal{F}} \rightarrow \mathbb{H}_{\mathcal{S}}$ as

$$\Pi_{\mathcal{F}}^{\mathcal{S}} u_{\mathcal{F}} := \sum_{\phi_i \in \mathcal{S}} u_i \phi_i, \quad (3)$$

that is, we extract the coefficients of $u_{\mathcal{F}}$ corresponding to the basis functions in \mathcal{S} , and we set the others to zero.

For any element K , we denote by \mathcal{R}_K the set of *removable* basis functions (see Section 2.1) associated to K , by $|\mathcal{R}_K|$ its cardinality, and by $\mathbb{H}_{\mathcal{R}_K}$ its associated space. Additionally, we define the subset of *essential* basis functions \mathcal{E}_K as $\mathcal{E}_K := \mathcal{F} \setminus \mathcal{R}_K$, while its associated space is denoted by $\mathbb{H}_{\mathcal{E}_K}$. These spaces satisfy that $\mathbb{H}_{\mathcal{E}_K} \subset \mathbb{H}_{\mathcal{F}}$, $\mathbb{H}_{\mathcal{R}_K} \subset \mathbb{H}_{\mathcal{F}}$, and $\mathbb{H}_{\mathcal{F}} = \mathbb{H}_{\mathcal{E}_K} \cup \mathbb{H}_{\mathcal{R}_K}$, with $\mathbb{H}_{\mathcal{E}_K} \cap \mathbb{H}_{\mathcal{R}_K} = \emptyset$. As a consequence, we can express any $u_{\mathcal{F}} \in \mathbb{H}_{\mathcal{F}}$, as:

$$u_{\mathcal{F}} = \Pi_{\mathcal{F}}^{\mathcal{E}_K} u_{\mathcal{F}} + \Pi_{\mathcal{F}}^{\mathcal{R}_K} u_{\mathcal{F}}. \quad (4)$$

Since we consider a single mesh at a time, the solution $u_{\mathcal{E}_K}$ in \mathcal{E}_K associated to Eq. (2) is, in fact, never computed. Instead, we employ the projection of $u_{\mathcal{F}}$ into \mathcal{E}_K to approximate it when necessary.

3.3. Error indicators

Let $\|\cdot\|_e$ be the *energy norm* associated to the Hilbert space \mathbb{H} . For elliptic problems (given by symmetric and positive-definite bilinear forms), we define this energy from the bilinear form of the problem b , that is, $\|\cdot\|_e^2 = b(\cdot, \cdot)$. For each non-elliptic problem, we shall define an alternative operator a –not necessarily a bilinear form– such that $|b(\phi, \psi)| \leq |a(\phi, \psi)| \quad \forall \phi, \psi \in \mathbb{H}$ and $\|\cdot\|_e^2 = a(\cdot, \cdot)$ is the energy norm of the problem. We stress that the choice of these operators might highly influence the results of the adaptive process, which is usually an essential ingredient of adaptive strategies.

With this in mind, our objective is to provide representative element-wise error indicators that drive the *hp*-coarsening steps (see Algorithm 2). For that, we consider isotropic and anisotropic indicators that are problem-dependent. In the following subsections, we derive only the isotropic error estimators $\eta_K, \forall K \in \mathcal{T}$ for a wide range of problems (see [25]. for anisotropic indicators).

To select what basis functions to unrefine, we compute the error indicators’ average (per degree of freedom), and we subsequently eliminate the *removable* basis function whose contribution is smaller than a percentage of this average. For further details and implementation technicalities, see [25].

In the following, we summarize the results from Darrigrand et al. [25] for elliptic energy-norm-based adaptive problems from the energy-norm perspective. After that, we extend these results to non-elliptic equations, and finally, we consider goal-oriented adaptivity applied to elliptic and non-elliptic problems. We can obtain all the proposed results by assuming (quasi)-*b*-orthogonality of the basis functions. However, this assumption is strong and unneeded for the energy-based adaptivity and, therefore, we only employ it for GOA.

To do so, let us denote by “ \lesssim ” the inequality that holds up to a constant; that is, we represent $a \lesssim Cb$ by $a \lesssim b$, with $a, b, C \in \mathbb{R}$, and let us define the L^2 -inner product of two possible complex and possibly vector valued functions g_1 and g_2 as:

$$\langle g_1, g_2 \rangle_{L^2(\Omega)} = \int_{\Omega} g_1^T g_2 \, d\Omega, \quad (5)$$

where g^T denotes the transpose of g .

3.3.1. Energy-norm based elliptic problems

For a given element $K \in \mathcal{T}$, the objective is to quantify how much energy we lose in the solution when removing a subset of basis functions of the set of removable basis functions \mathcal{R}_K . Specifically, we want to compute $\|u_{\mathcal{F}} - u_{\mathcal{E}_K}\|_e^2$. If this quantity is small, we guarantee that the energy of the removed set of basis functions is insignificant. Therefore, the fine and the unrefined meshes would provide comparable results.

Analogously to Cea’s lemma proof, we derive:

$$\|u_{\mathcal{F}} - u_{\mathcal{E}_K}\|_e^2 = b(u_{\mathcal{F}} - u_{\mathcal{E}_K}, u_{\mathcal{F}} - u_{\mathcal{E}_K}) \quad (6)$$

$$= b(u_{\mathcal{F}} - u_{\mathcal{E}_K}, u_{\mathcal{F}} - \Pi_{\mathcal{F}}^{\mathcal{E}_K} u_{\mathcal{F}}) + b(u_{\mathcal{F}} - u_{\mathcal{E}_K}, \Pi_{\mathcal{F}}^{\mathcal{E}_K} u_{\mathcal{F}} - u_{\mathcal{E}_K}) \quad (7)$$

$$\leq \|u_{\mathcal{F}} - u_{\mathcal{E}_K}\|_e \left\| u_{\mathcal{F}} - \Pi_{\mathcal{F}}^{\mathcal{E}_K} u_{\mathcal{F}} \right\|_e, \quad (8)$$

where we have used the b -orthogonality of $u_{\mathcal{F}} - u_{\mathcal{E}_K}$ with $\mathbb{H}_{\mathcal{E}_K}$ and the Cauchy-Schwarz inequality. Therefore,

$$\|u_{\mathcal{F}} - u_{\mathcal{E}_K}\|_e \leq \left\| u_{\mathcal{F}} - \Pi_{\mathcal{F}}^{\mathcal{E}_K} u_{\mathcal{F}} \right\|_e = \left\| \Pi_{\mathcal{F}}^{\mathcal{R}_K} u_{\mathcal{F}} \right\|_e. \quad (9)$$

It is then natural to define the following element-wise error indicator:

$$\eta_K := \left\| \Pi_{\mathcal{F}}^{\mathcal{R}_K} u_{\mathcal{F}} \right\|_e^2, \quad \forall K \in \mathcal{T}. \quad (10)$$

3.3.2. Extension to energy-based non-elliptic problems

Again, our purpose is to compute $\|u_{\mathcal{F}} - u_{\mathcal{E}_K}\|_e^2$ to eliminate the removable basis functions with low contribution to the solution. For that, let us start with the triangular inequality, which provides that

$$\|u_{\mathcal{F}} - u_{\mathcal{E}_K}\|_e \leq \left\| u_{\mathcal{F}} - \Pi_{\mathcal{F}}^{\mathcal{E}_K} u_{\mathcal{F}} \right\|_e + \left\| \Pi_{\mathcal{F}}^{\mathcal{E}_K} u_{\mathcal{F}} - u_{\mathcal{E}_K} \right\|_e. \quad (11)$$

Let us assume now that b satisfies the discrete inf-sup condition:

$$\exists \gamma > 0, \quad \inf_{\phi \in \mathbb{H}_{\mathcal{E}_K}} \sup_{\psi \in \mathbb{H}_{\mathcal{E}_K}} \frac{b(\phi, \psi)}{\|\phi\|_e \|\psi\|_e} \geq \gamma. \quad (12)$$

Then, using this inequality and the b -orthogonality of $u_{\mathcal{F}} - u_{\mathcal{E}_K}$ with respect to $\mathbb{H}_{\mathcal{E}_K}$, we control the second term of Eq. (11):

$$\gamma \left\| \Pi_{\mathcal{F}}^{\mathcal{E}_K} u_{\mathcal{F}} - u_{\mathcal{E}_K} \right\|_e \leq \sup_{\psi \in \mathbb{H}_{\mathcal{E}_K}} \frac{b(\Pi_{\mathcal{F}}^{\mathcal{E}_K} u_{\mathcal{F}} - u_{\mathcal{E}_K}, \psi)}{\|\psi\|_e} \quad (13)$$

$$\leq \sup_{\psi \in \mathbb{H}_{\mathcal{E}_K}} \frac{b(\Pi_{\mathcal{F}}^{\mathcal{E}_K} u_{\mathcal{F}} - u_{\mathcal{F}}, \psi) + b(u_{\mathcal{F}} - u_{\mathcal{E}_K}, \psi)}{\|\psi\|_e} \quad (14)$$

$$\leq \sup_{\psi \in \mathbb{H}_{\mathcal{E}_K}} \frac{M_b \left\| \Pi_{\mathcal{F}}^{\mathcal{E}_K} u_{\mathcal{F}} - u_{\mathcal{F}} \right\|_e \|\psi\|_e}{\|\psi\|_e} \quad (15)$$

$$\leq M_b \left\| u_{\mathcal{F}} - \Pi_{\mathcal{F}}^{\mathcal{E}_K} u_{\mathcal{F}} \right\|_e, \quad (16)$$

where M_b is the continuity constant of b . Therefore,

$$\|u_{\mathcal{F}} - u_{\mathcal{E}_K}\|_e^2 \lesssim \left\| u_{\mathcal{F}} - \Pi_{\mathcal{F}}^{\mathcal{E}_K} u_{\mathcal{F}} \right\|_e^2 = \left\| \Pi_{\mathcal{F}}^{\mathcal{R}_K} u_{\mathcal{F}} \right\|_e^2. \quad (17)$$

Accordingly, we define the element-wise indicator as:

$$\eta_K := \left\| \Pi_{\mathcal{F}}^{\mathcal{R}_K} u_{\mathcal{F}} \right\|_e^2, \quad \forall K \in \mathcal{T}. \quad (18)$$

The coarsening step will unrefine the elements that exhibit small η_K . Therefore, Eq. (17) ensures that the loss in the energy of the problem will be negligible when removing these basis functions.

3.3.3. Extension to goal-oriented adaptivity

GOA techniques aim to approximate specific quantities of finite element solutions rather than the global energy of the problem. These quantities with particular engineering applications are often called influence functions or QoIs. Thus, the objective is to produce a space $\mathbb{H}_{\mathcal{F}}$ with a minimum dimension such that the error in the QoI is below a user-prescribed tolerance. To control the error in the QoI, we introduce the following adjoint problem [33,34] associated to Eq. (1):

$$\left| \begin{array}{l} \text{Find } v \in \mathbb{H} \text{ such that} \\ b(\phi, v) = l(\phi), \quad \forall \phi \in \mathbb{H}, \end{array} \right. \quad (19)$$

where $l : \mathbb{H} \rightarrow \mathbb{R}$ is a linear continuous form. Hence, the QoI of the solution $u_{\mathcal{F}}$ is denoted by $l(u_{\mathcal{F}})$. The discrete equivalent of this problem is given by:

$$\left| \begin{array}{l} \text{Find } v_{\mathcal{F}} \in \mathbb{H}_{\mathcal{F}} \text{ such that} \\ b(\phi_{\mathcal{F}}, v_{\mathcal{F}}) = l(\phi_{\mathcal{F}}), \quad \forall \phi_{\mathcal{F}} \in \mathbb{H}_{\mathcal{F}}, \end{array} \right. \quad (20)$$

where $v_{\mathcal{F}}$ stands for the Galerkin approximation of the solution v to the adjoint problem associated with the space $\mathbb{H}_{\mathcal{F}}$. For the mathematical analysis, we also consider the solution $v_{\mathcal{E}_K}$ in \mathcal{E}_K associated with Eq. (20), although we never compute it in practice.

For a given element $K \in \mathcal{T}$, we want to quantify how much the QoI changes when removing some basis functions from the set of removable basis functions \mathcal{R}_K associated with K . That is, we need to control $|l(u_{\mathcal{F}}) - l(u_{\mathcal{E}_K})| \quad \forall K \in \mathcal{T}$.

Since $\mathbb{H}_{\mathcal{E}_K} \subset \mathbb{H}_{\mathcal{F}}$, Galerkin orthogonality ensures that

$$b(u_{\mathcal{F}} - u_{\mathcal{E}_K}, \phi) = 0, \quad \forall \phi \in \mathbb{H}_{\mathcal{E}_K}. \quad (21)$$

Then,

$$l(u_{\mathcal{F}}) - l(u_{\mathcal{E}_K}) = b(u_{\mathcal{F}} - u_{\mathcal{E}_K}, v_{\mathcal{F}}) = b(u_{\mathcal{F}} - u_{\mathcal{E}_K}, v_{\mathcal{F}} - v_{\mathcal{E}_K}). \quad (22)$$

Using Eq. (4) on $v_{\mathcal{F}}$, we have that:

$$l(u_{\mathcal{F}}) - l(u_{\mathcal{E}_K}) = b(u_{\mathcal{F}} - u_{\mathcal{E}_K}, \Pi_{\mathcal{F}}^{\mathcal{R}_K} v_{\mathcal{F}} + \Pi_{\mathcal{F}}^{\mathcal{E}_K} v_{\mathcal{F}} - v_{\mathcal{E}_K}) \quad (23)$$

$$= b(u_{\mathcal{F}} - u_{\mathcal{E}_K}, \Pi_{\mathcal{F}}^{\mathcal{R}_K} v_{\mathcal{F}}) + b(u_{\mathcal{F}} - u_{\mathcal{E}_K}, \Pi_{\mathcal{F}}^{\mathcal{E}_K} v_{\mathcal{F}} - v_{\mathcal{E}_K}). \quad (24)$$

Again, thanks to Galerkin orthogonality the second term vanishes. Then, applying Eq. (4) on $u_{\mathcal{F}}$ to the remaining term, we have that

$$l(u_{\mathcal{F}}) - l(u_{\mathcal{E}_K}) = b(\Pi_{\mathcal{F}}^{\mathcal{R}_K} u_{\mathcal{F}} + \Pi_{\mathcal{F}}^{\mathcal{E}_K} u_{\mathcal{F}} - u_{\mathcal{E}_K}, \Pi_{\mathcal{F}}^{\mathcal{R}_K} v_{\mathcal{F}}) \quad (25)$$

$$= b(\Pi_{\mathcal{F}}^{\mathcal{R}_K} u_{\mathcal{F}}, \Pi_{\mathcal{F}}^{\mathcal{R}_K} v_{\mathcal{F}}) + b(\Pi_{\mathcal{F}}^{\mathcal{E}_K} u_{\mathcal{F}} - u_{\mathcal{E}_K}, \Pi_{\mathcal{F}}^{\mathcal{R}_K} v_{\mathcal{F}}). \quad (26)$$

Additionally, if we assume that \mathcal{E}_K is (quasi) b -orthogonal to \mathcal{R}_K due to the (quasi)-orthogonality assumption of the basis functions, then

$$b(\Pi_{\mathcal{F}}^{\mathcal{E}_K} u_{\mathcal{F}} - u_{\mathcal{E}_K}, \Pi_{\mathcal{F}}^{\mathcal{R}_K} v_{\mathcal{F}}) \simeq 0, \quad (27)$$

and consequently,

$$|l(u_{\mathcal{F}}) - l(u_{\mathcal{E}_K})| \simeq |b(\Pi_{\mathcal{F}}^{\mathcal{R}_K} u_{\mathcal{F}}, \Pi_{\mathcal{F}}^{\mathcal{R}_K} v_{\mathcal{F}})| \leq |a(\Pi_{\mathcal{F}}^{\mathcal{R}_K} u_{\mathcal{F}}, \Pi_{\mathcal{F}}^{\mathcal{R}_K} v_{\mathcal{F}})|. \quad (28)$$

Then, we define the element-wise indicators as

$$\eta_K := \left| a(\Pi_{\mathcal{F}}^{\mathcal{R}_K} u_{\mathcal{F}}, \Pi_{\mathcal{F}}^{\mathcal{R}_K} v_{\mathcal{F}}) \right|, \quad \forall K \in \mathcal{T}. \quad (29)$$

Here again, Eq. (28) ensures that eliminating the basis functions associated with small indicators during the coarsening process should have a limited effect on the error of the QoI.

Remark. Since b is continuous on \mathbb{H} with respect to the energy norm, we also have

$$|l(u_{\mathcal{F}}) - l(u_{\mathcal{E}_K})| \simeq \left| b(\Pi_{\mathcal{F}}^{\mathcal{R}_K} u_{\mathcal{F}}, \Pi_{\mathcal{F}}^{\mathcal{R}_K} v_{\mathcal{F}}) \right| \lesssim \left\| \Pi_{\mathcal{F}}^{\mathcal{R}_K} u_{\mathcal{F}} \right\|_e \left\| \Pi_{\mathcal{F}}^{\mathcal{R}_K} v_{\mathcal{F}} \right\|_e, \quad (30)$$

and we could also define the element-wise indicators based on the above equation. Notice that if we select l to be the source term in the adjoint problem defined by Eq. (19), with Eq. (30) we recover the element-wise indicators derived previously in Eqs. (10) and (18). However, in the forthcoming numerical results, we employ the estimators based on Eq. (29).

4. Numerical results

This section illustrates the performance of our hp -adaptive strategy for a wide range of problems. We solve 2D elliptic and non-elliptic problems based on Poisson, Helmholtz, and convection–diffusion equations exhibiting multiple singularities. Additionally, we solve a 3D non-elliptic problem based on a heterogeneous Helmholtz’s equation. For each example, we first display the results associated with the energy-norm adaptivity, followed by GOA results. For all the experiments, we consider the Hilbert space $\mathbb{H} = \{u \in H^1(\Omega) \mid u = 0 \text{ on } \Gamma_D\}$, where Ω is the computational domain, and display the final adapted h - and hp -meshes and the convergence curves for hp -adaptivity and h -adaptivity with uniform $p = 1$ and $p = 2$. All the experiments start with a coarse mesh that is conforming to the materials and the source.

We refer to u as the solution in a fine grid, while $u_{\mathcal{T}_c}$ is the solution associated with a coarser unrefined mesh. In energy-norm adaptivity, we define the relative error in percentage as:

$$e_{\text{rel}}^{\text{energy}} := \frac{\|u - u_{\mathcal{T}_c}\|_{\mathbb{H}}}{\|u\|_{\mathbb{H}}} \cdot 100. \quad (31)$$

Rather than maintaining several grids, our easy-to-implement approach only stores a single grid at a time. Thus, we estimate the following lower bound of the error $e_{\text{rel}}^{\text{energy}}$ as follows:

$$\tilde{e}_{\text{rel}}^{\text{energy}} := \frac{|\|u\|_{\mathbb{H}} - \|u_{\mathcal{T}_c}\|_{\mathbb{H}}|}{\|u\|_{\mathbb{H}}} \cdot 100 \leq e_{\text{rel}}^{\text{energy}}. \quad (32)$$

We define the relative error in a QoI in percentage as follows:

$$e_{\text{rel}}^{\text{QoI}} := \frac{|l(u) - l(u_{\mathcal{T}_c})|}{|l(u)|} \cdot 100. \quad (33)$$

In some cases where the exact solution is available, we will replace the fine grid solution u with the exact solution, and we will directly compute $e_{\text{rel}}^{\text{energy}}$ and $e_{\text{rel}}^{\text{QoI}}$.

For the GOA problems, we define our QoI as

$$l(\phi) = \frac{1}{|\Omega_l|} \langle \mathbb{1}_{\Omega_l}, \phi \rangle_{L^2(\Omega)}, \quad \forall \phi \in \mathbb{H}, \quad (34)$$

where $|\Omega_l|$ defines the area or volume of Ω_l and $\mathbb{1}_{\Omega_l}$ is a function equal to one if $x \in \Omega_l$, and zero otherwise.

4.1. Singular Poisson example

We consider the following elliptic problem based on the Poisson equation.

$$\begin{array}{|l} \text{Find } u \text{ such that} \\ -\Delta u = \mathbb{1}_{\Omega_f} \text{ in } \Omega, \\ u = 0 \quad \text{on } \partial\Omega, \end{array} \quad \begin{array}{l} (35) \\ (36) \end{array}$$

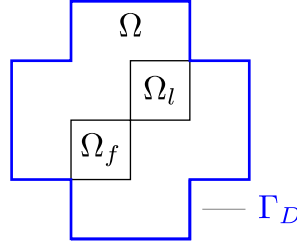


Fig. 3. Domain for our Poisson example. Γ_D denotes the Dirichlet boundary, Ω is the domain, Ω_l denotes the support of the QoI $l(\phi)$, and Ω_f is the support of the source function.

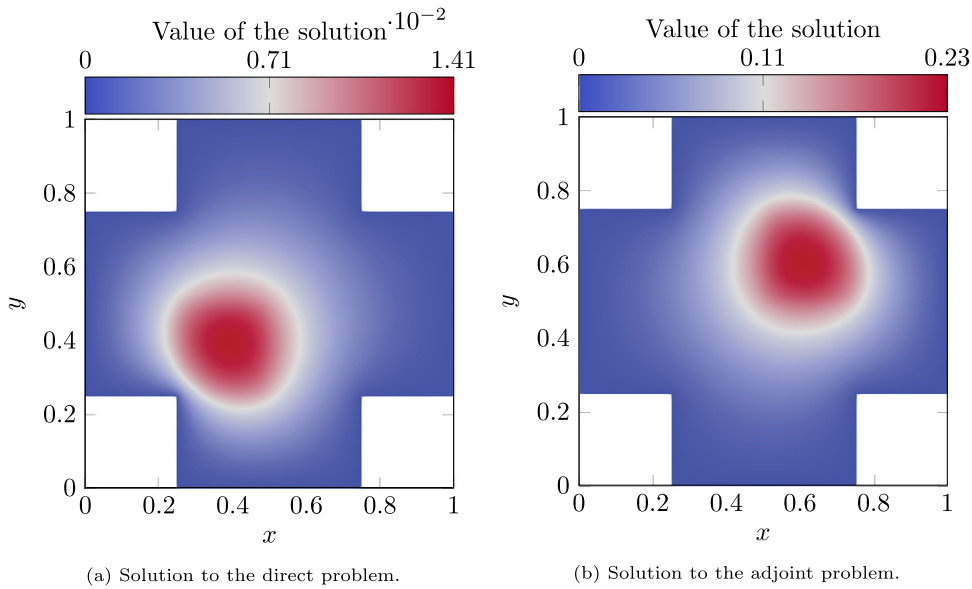


Fig. 4. Direct and adjoint solutions of our singular Poisson example.

where $\Omega = (0, 1) \times (\frac{1}{4}, \frac{3}{4}) \cup (\frac{1}{4}, \frac{3}{4}) \times (0, 1) \subset \mathbb{R}^2$ and $\Omega_f = (\frac{1}{4}, \frac{1}{2})^2 \subset \Omega$. Following the definition of Eq. (34) for the QoI, we select $\Omega_l = (\frac{1}{2}, \frac{3}{4})^2 \subset \Omega$. Fig. 3 shows the domain Ω of this elliptic problem. For elliptic problems in energy-norm adaptivity, we refer the interested reader to [25]. For goal-oriented adaptivity, Figs. 4a and 4b show the solutions of the direct and adjoint problems, respectively.

We define the operators $b(\cdot, \cdot)$ and $a(\cdot, \cdot)$ associated with the above problem as follows:

$$b(\cdot, \cdot) := \langle \nabla \cdot, \nabla \cdot \rangle_{L^2(\Omega)}, \quad (37)$$

and $a(\cdot, \cdot) = b(\cdot, \cdot)$.

Fig. 5 shows the final h - and hp -adapted meshes and the evolution of $e_{\text{rel}}^{\text{QoI}}$. The first uniform mesh is composed of twelve root elements: given an initial 4×4 grid over a square domain, we have removed the four corner elements. The grid adapts to the four localized reentrant corners of the domain. The hp -adaptive strategy performs h -refinements near these singularities and p -refinement as we move away from them, as physically expected. We also observe heavy refinements around the central point of the domain. That is the only point where the right-hand sides of the direct and adjoint problems are discontinuous; therefore, solutions of the direct and adjoint problems simultaneously exhibit low regularity (only H^2). Consequently, some refinements there are expected. Convergence rates of the proposed hp -adaptive strategy are quasi-optimal (see Fig. 5d).

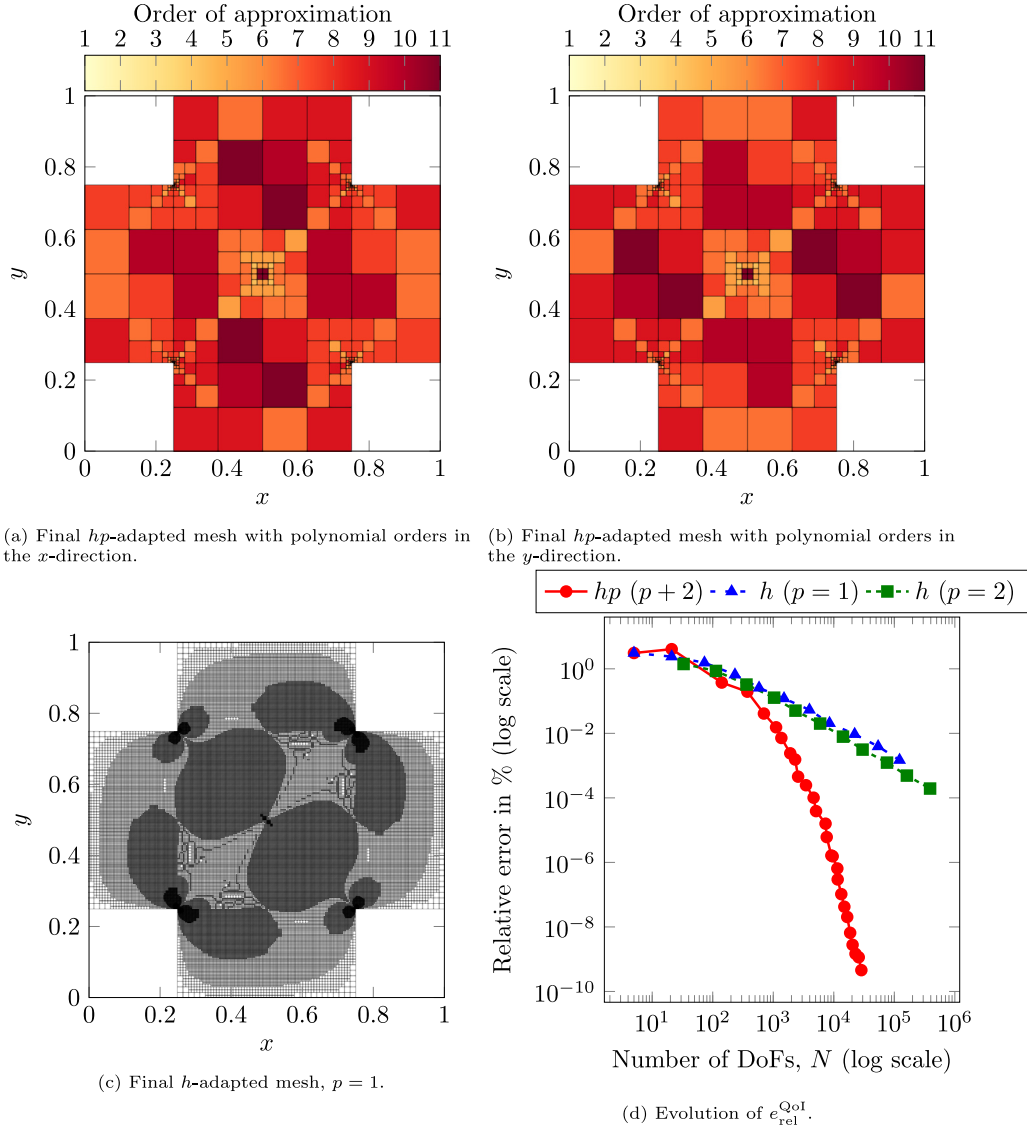


Fig. 5. Final h - and hp -adapted meshes for our singular Poisson example and evolution of $e_{\text{rel}}^{\text{QoI}}$.

4.2. Wave propagation problem

We consider the following non-elliptic problem based on Helmholtz's equation.

Find u such that,

$$-\Delta u - k^2 u = \mathbb{1}_{\Omega_f} \quad \text{in } \Omega, \quad (38)$$

$$u = 0 \quad \text{on } \Gamma_D, \quad (39)$$

$$\nabla u \cdot \vec{n} = 0 \quad \text{on } \Gamma_N, \quad (40)$$

where $\Omega = (0, 1)^2 \setminus (\frac{1}{4}, \frac{3}{4})^2 \subset \mathbb{R}^2$, $\Omega_f = (0, \frac{1}{4})^2 \subset \Omega$, and $k = (8 \cdot 2\pi, 2\pi)$. The complex-valued k indicates the medium is lossy. Γ_D and Γ_N stand for the parts of the boundary $\partial\Omega$ where we impose homogeneous Dirichlet and

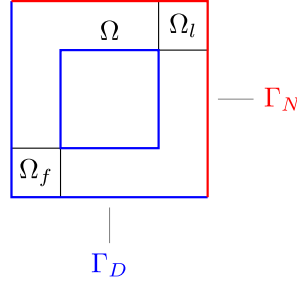


Fig. 6. Domain for our wave propagation problem. Γ_D denotes the Dirichlet boundary, Γ_N stands for the Neumann boundary, Ω is the domain, Ω_l is the support of the QoI $l(\phi)$, and Ω_f is the support of the source function.

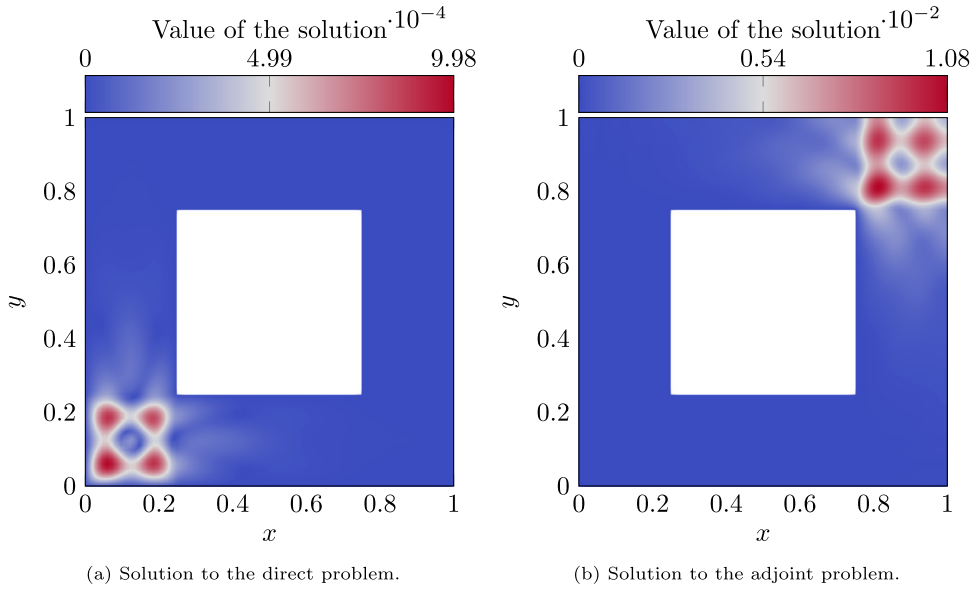


Fig. 7. Absolute value of the direct and adjoint solutions of our wave propagation example in a lossy medium.

Neumann boundary conditions, respectively. From Eq. (34), we define $\Omega_l = (\frac{3}{4}, 1)^2 \subset \Omega$. Fig. 6 shows the domain of this non-elliptic problem.

We define the operators $b(\cdot, \cdot)$ and $a(\cdot, \cdot)$ associated with the above problem as follows:

$$b(\cdot, \cdot) := \langle \nabla \cdot, \nabla \cdot \rangle_{L^2(\Omega)} - k^2 \langle \cdot, \cdot \rangle_{L^2(\Omega)}, \quad a(\cdot, \cdot) := |\langle \nabla \cdot, \nabla \cdot \rangle_{L^2(\Omega)}| + |k^2| |\langle \cdot, \cdot \rangle_{L^2(\Omega)}|. \quad (41)$$

Once more, $\|\cdot\|_e^2 = a(\cdot, \cdot)$ defines our energy norm and $|b(\phi, \psi)| \leq |a(\phi, \psi)|$, $\forall \phi, \psi \in \mathbb{H}$.

4.2.1. Energy-norm adaptivity

For goal-oriented adaptivity, Figs. 7a and 7b show the solutions to the direct and adjoint problems, respectively. Fig. 8 shows the final h - and hp -adapted meshes and Fig. 9 shows the evolution of $\tilde{e}_{\text{rel}}^{\text{energy}}$ and $e_{\text{rel}}^{\text{QoI}}$. The initial uniform mesh is composed of twelve root elements. We perform a double h -hierarchical refinement on the initial mesh to obtain a fine mesh to start the adaptivity.

For the h -adapted case, we observe heavy refinements around the source; however, almost no refinement occurs near the QoI. That happens due to the lossy nature of the problem. As a result, we observe a proper energy-norm convergence, as shown in Fig. 9a, but a poor convergence behavior in the QoI, as demonstrated in Fig. 9b.

When executing the hp -adaptive strategy, we again observe heavier refinements around the source than in the vicinity of the QoI. However, because of the fast convergence of the hp -adaptivity, some non-trivial refinements

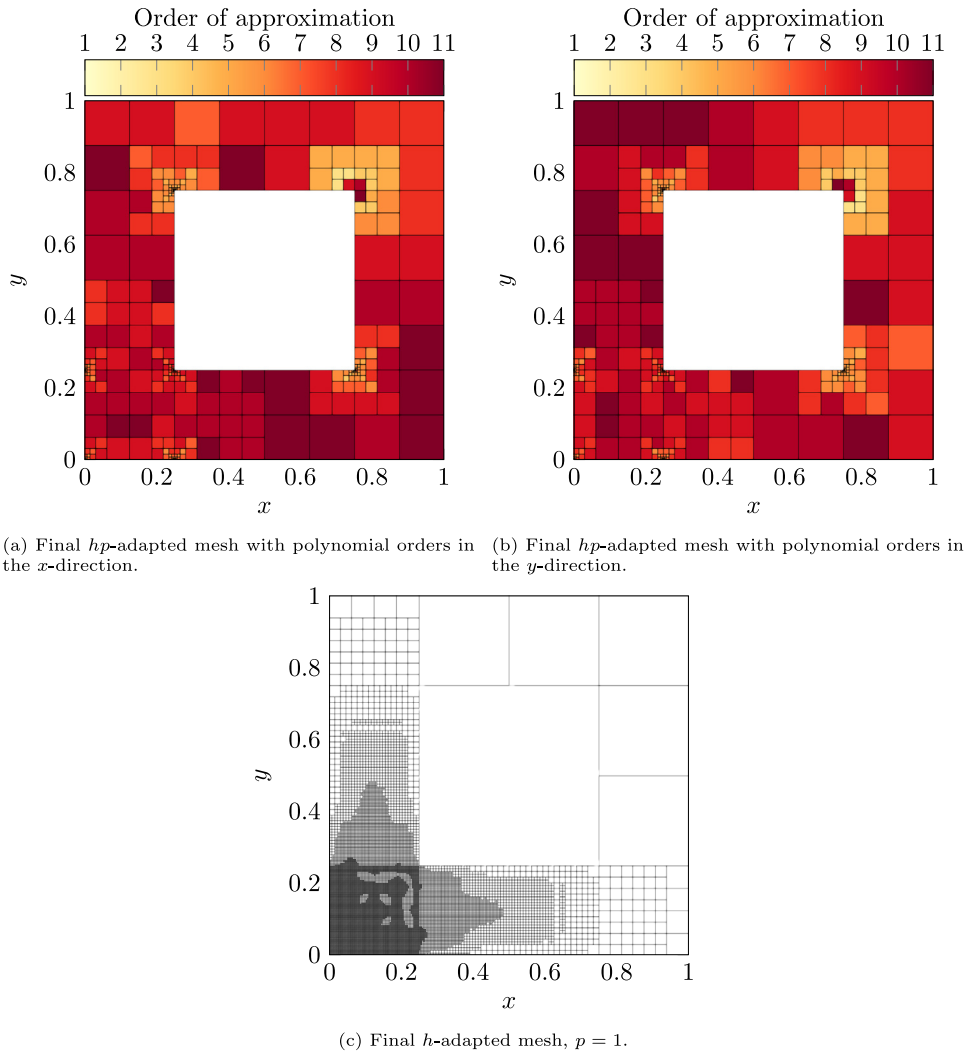


Fig. 8. Final h - and hp -adapted meshes for our wave propagation example in a lossy medium.

still occur around the QoI. As a result, the relative error in the QoI $e_{\text{rel}}^{\text{QoI}}$ also converges up to the level of $10^{-3}\%$ for 20k unknowns.

4.2.2. Goal-oriented adaptivity

Fig. 10 shows the final h - and hp -adapted meshes and the evolution of $e_{\text{rel}}^{\text{QoI}}$. The initial mesh is uniform and composed of twelve root elements. As in the energy-norm adaptivity, we perform a double h -hierarchical refinement on the initial mesh to obtain a fine mesh to start the adaptivity. We observe heavy h -refinements around four localized singularities at the interior corners of the domain. In addition, we recover exponential convergence rates for the h - and for the hp -adaptive versions. As a result, we construct a hp -adapted mesh with 20k unknowns that delivers a relative error in the QoI of $10^{-6}\%$ (three orders of magnitude better than in Fig. 9b).

To better illustrate this idea, Fig. 11 compares the evolution of $e_{\text{rel}}^{\text{QoI}}$ and $\tilde{e}_{\text{rel}}^{\text{energy}}$ when executing the energy-norm and the goal-oriented hp -adaptive strategies in our wave propagation example in a lossy medium. Fig. 11(a) shows a relative error in the QoI three orders of magnitude better when performing goal-oriented adaptivity than considering energy-norm adaptivity. Fig. 11(b) shows that the $\tilde{e}_{\text{rel}}^{\text{energy}}$ rapidly converges when employing energy-norm adaptivity, while with the hp -adaptive GOA strategy, the rapid initial convergence stagnates at the level of $10^{-6}\%$. As expected, this situation is also noticeable in terms of h -adaptivity (see Figs. 9 and 10d).

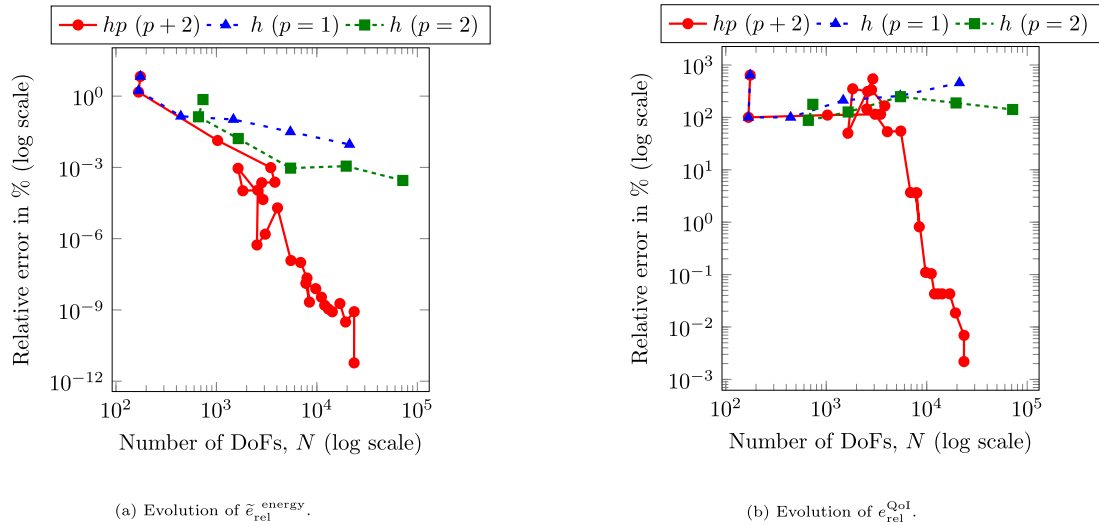


Fig. 9. Energy-norm adaptivity. Evolution of \tilde{e}_{rel}^{energy} and e_{rel}^{QoI} in our wave propagation example in a lossy medium.

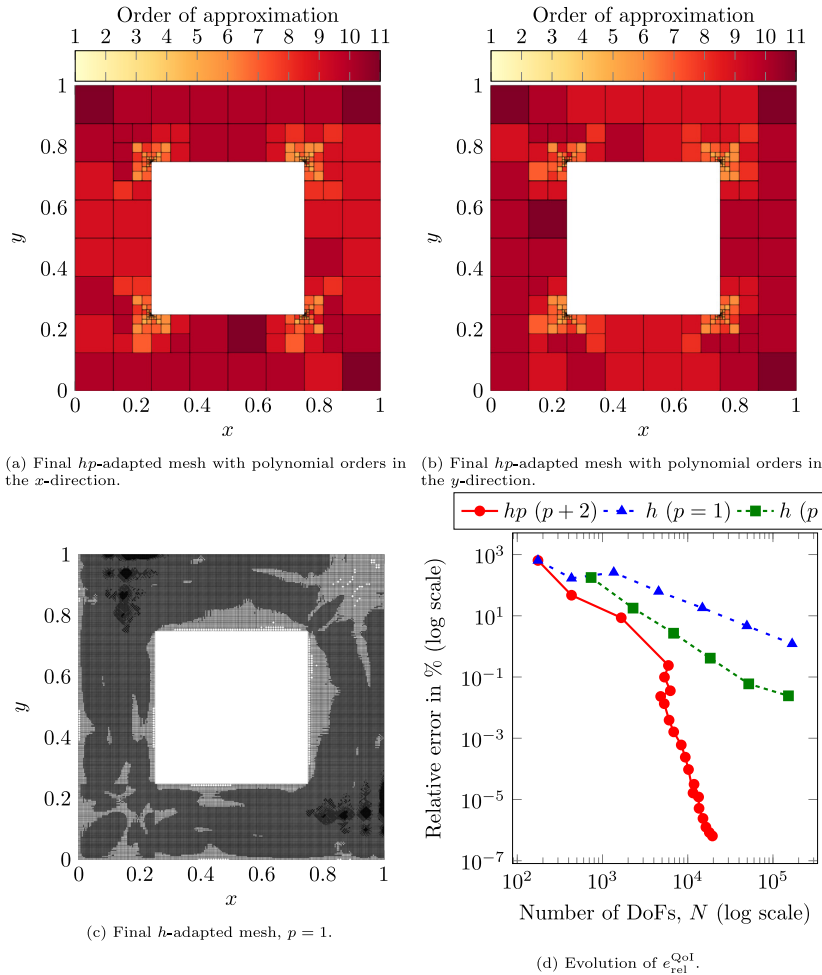


Fig. 10. Final h - and hp -adapted meshes for our singular goal-oriented wave propagation example in a lossy medium and the evolution of e_{rel}^{QoI} .

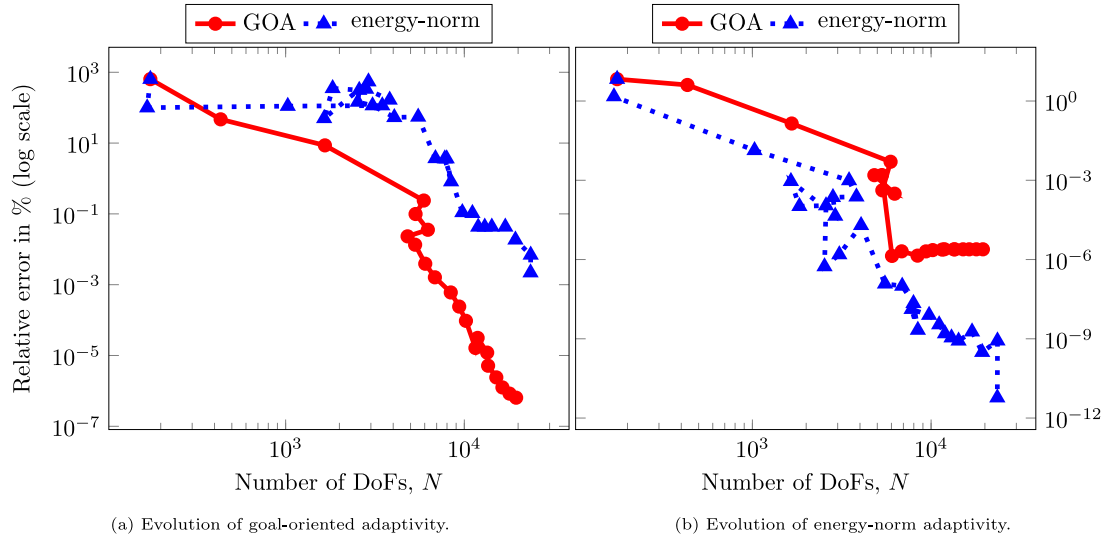


Fig. 11. Convergence history of $e_{\text{rel}}^{\text{QoI}}$ and $z_{\text{rel}}^{\text{energy}}$ for the energy-norm and GOA hp -adaptive strategies.

4.3. Convection-dominated diffusion : example 1

We consider the following non-elliptic problem based on the convection-dominated diffusion equation.

$$\left\{ \begin{array}{l} \text{Find } u \text{ such that,} \\ -\varepsilon \Delta u + \sigma \cdot \nabla u = f \text{ in } \Omega, \\ u = 0 \text{ on } \partial\Omega. \end{array} \right. \quad (42)$$

The selection of a suitable norm to measure the error in problems based on (42) is an open research subject. For instance, authors of [58,59] use the standard energy norm, in [60] a balanced norm, and in [61,62] different norms from the previous ones. In here, we define the operators $b(\cdot, \cdot)$ and $a(\cdot, \cdot)$ associated with the above problem as follows:

$$b(\cdot, \cdot) := \varepsilon \langle \nabla \cdot, \nabla \cdot \rangle_{L^2(\Omega)} + \langle \sigma \nabla \cdot, \cdot \rangle_{L^2(\Omega)}, \quad a(\cdot, \cdot) := (\varepsilon + C) \langle \nabla \cdot, \nabla \cdot \rangle_{L^2(\Omega)}, \quad (43)$$

where $\|\cdot\|_e^2 = a(\cdot, \cdot)$ is our energy norm and $C \in \mathbb{R}^+$. We select this definition of $a(\cdot, \cdot)$ by bounding from above the convective term of $b(\cdot, \cdot)$ using a mesh-independent constant C for the Poincaré inequality that also includes the effect of σ ^{1,2}.

4.3.1. Energy-norm adaptivity

For this example, we consider $\varepsilon = 10^{-3}$ as the diffusive coefficient, $\sigma = (3, 1)^T$, and $\Omega = (0, 1)^2$. The load function f is a linear continuous form on \mathbb{H} and it is selected so that the solution u is of the form:

$$u(x, y) = e^{\frac{\varepsilon}{x(x-1)}} \cosh\left(500\left(\frac{1}{2} + \sigma^{-1}(x, -y)\right)\right)^{-2}. \quad (44)$$

Fig. 12 shows the solution of this convection-dominated diffusion example. The initial uniform mesh is composed of thirty-six root elements. Fig. 13 shows the final energy-norm h - and hp -adapted meshes and the evolution of e_{rel} . As expected, we observe heavy h -refinements around the line that characterizes the solution. In the hp -adapted case, we also observe an increase in the polynomial order in some of the elements near this characteristic line. We also observe exponential convergence rates (see Fig. 13d).

¹ It is essential to consider a mesh-independent norm $a(\cdot, \cdot)^{1/2}$ since we approximate some errors by computing the difference of the norm of two approximated solutions evaluated on *different* grids.

² The actual value of the constant C is unneeded in practice since we compute relative error indicators; in our case, we select $(C + \varepsilon) = 1$.

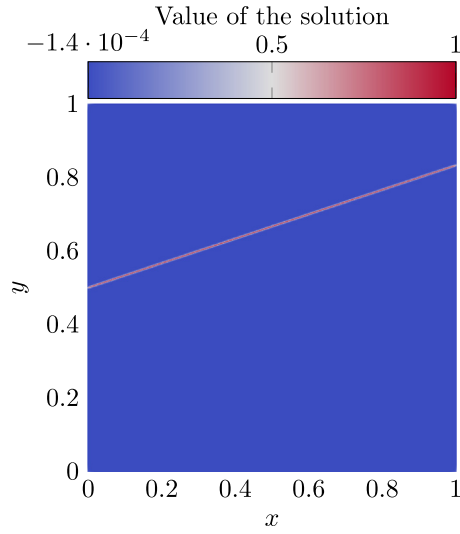


Fig. 12. Solution of the convection-dominated diffusion example 1.

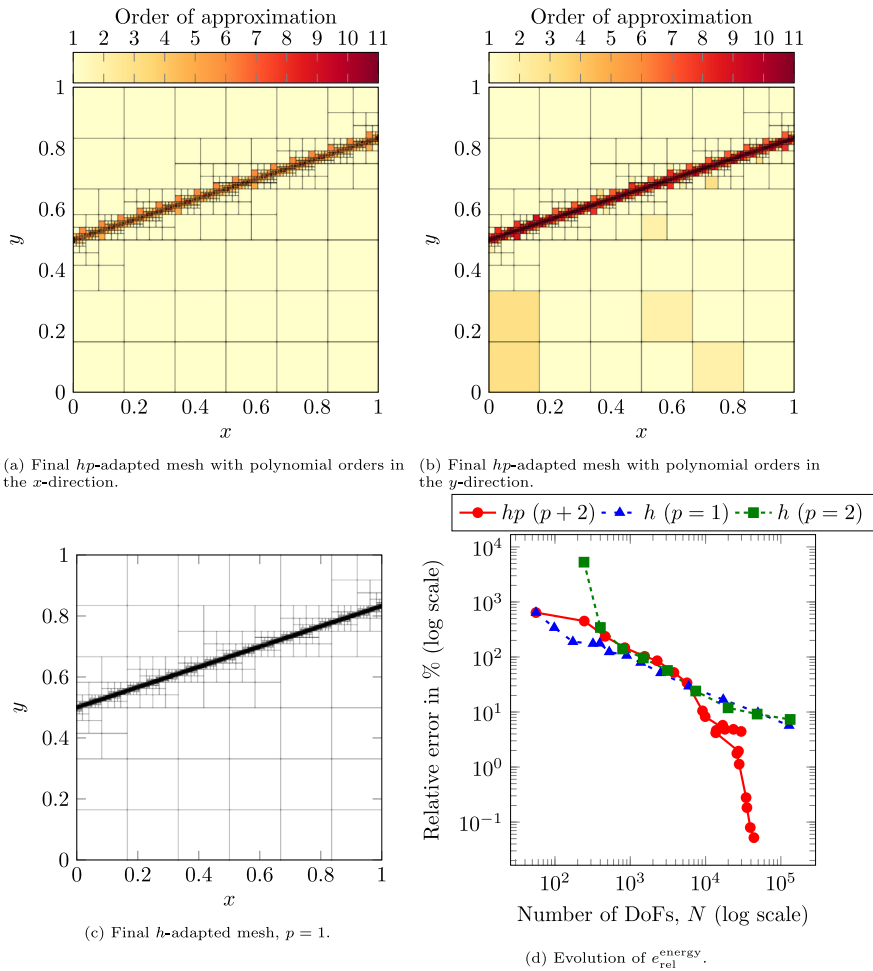


Fig. 13. Final h - and hp -adapted meshes for our convection-dominated diffusion example and the evolution of e_{rel}^{energy} .

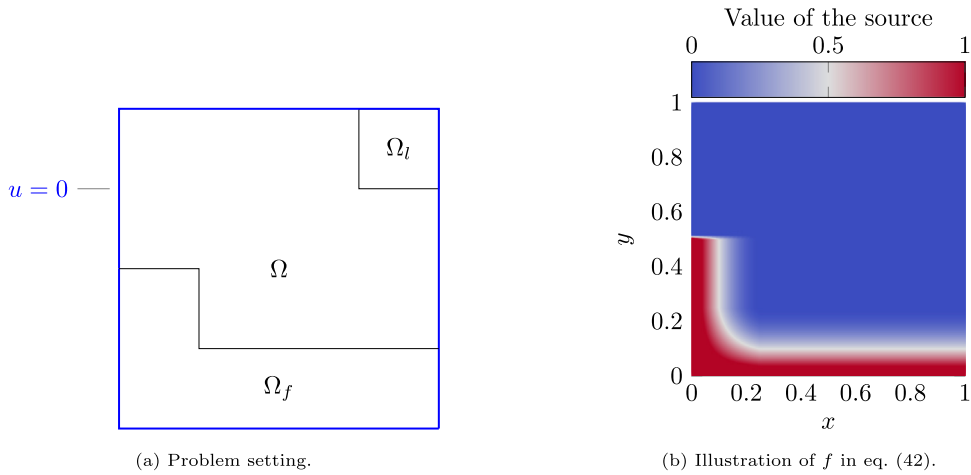


Fig. 14. Problem description for our second convection-dominated diffusion with advection skew to the mesh.

4.4. Convection-dominated diffusion : example 2

We now consider a more challenging setting with advection skew to the mesh. We solve a similar problem to the one depicted in Figure 9.3 of [63] (see Fig. 14). Our convection-dominated diffusion problem is governed by Eq. (42) on the domain $\Omega = (0, 1)^2$, with $\varepsilon = 10^{-4}$, $\sigma = (\cos \theta, \sin \theta)^T$, $\theta = \arctan(2)$, and zero Dirichlet boundary conditions, as depicted in Fig. 14(a).

We define our source term f (with support in Ω_f and illustrated in Fig. 14(b)) as:

$$f(x, y) = \begin{cases} (1 - 4x)^2, & \text{if } x \in [0, 0.25], y \in [0.25, 0.5], \\ (1 - 4y)^2, & \text{if } x \in [0.25, 1], y \in [0, 0.25], \\ (1 - 4x)(1 - 4y) + (1 - 4y)^2 4x + (1 - 4x)^2 4y, & \text{if } x \in [0, 0.25], y \in [0, 0.25], \\ 0, & \text{otherwise.} \end{cases} \quad (45)$$

Both the problem of Figure 9.3 of [63] and our problem share a strong boundary layer along the top and right boundaries of the domain. In addition, our problem incorporates (a) a source discontinuity on the edge $0 \leq x \leq 0.25$, $y = 0.5$ that is visible in Fig. 14(b), and (b) a strong boundary layer for the adjoint problem along the bottom border of the domain. Thus, our example exhibits strong gradients of different (unknown) intensities in various areas of the domain, which makes it ideal for assessing the performance of our proposed hp -adaptive algorithm. The initial uniform mesh consists of 4×4 root elements for both adaptive strategies.

4.4.1. Energy-norm adaptivity

Fig. 15 displays the final solution of the convection-dominated diffusion example 2 for the energy-norm adaptivity. Fig. 16 shows the final energy-norm h - and hp -adapted meshes and the evolution of the relative error when using energy-norm adaptivity. As expected, h and hp meshes exhibit strong h -refinements towards the two boundary layers on the top and right sides of the domain. In addition, the hp -adaptivity is also able to capture both the advection propagation direction and the source discontinuity.

Figs. 17 and 18 illustrate the evolution of the energy-based adaptive process by displaying at different iterations several solutions to the problem (left panels) and their corresponding hp -adaptive meshes (right panels). These meshes only display the polynomial orders in the x -direction, but analogous results are obtained for the y -direction. We accentuate the capability of the proposed algorithm to eliminate degrees of freedom previously introduced during the pre-asymptotic regime due to spurious oscillations. For instance, at iteration 7 (Fig. 17b), high polynomial orders p are set on the center-right part of the domain to capture the numerical artifacts exhibited by the solution (Fig. 17a). Once we better solve the problem, the numerical pollution starts to vanish (Fig. 17c), and consequently, some previously introduced high-order elements are p -unrefined (see Fig. 17d) on the elements near the center of the domain and close to the right boundary layer.

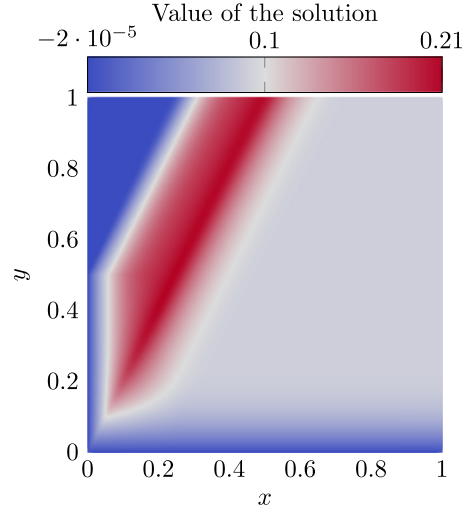


Fig. 15. Numerical solution of the convection-dominated diffusion example 2 for energy-norm adaptivity.

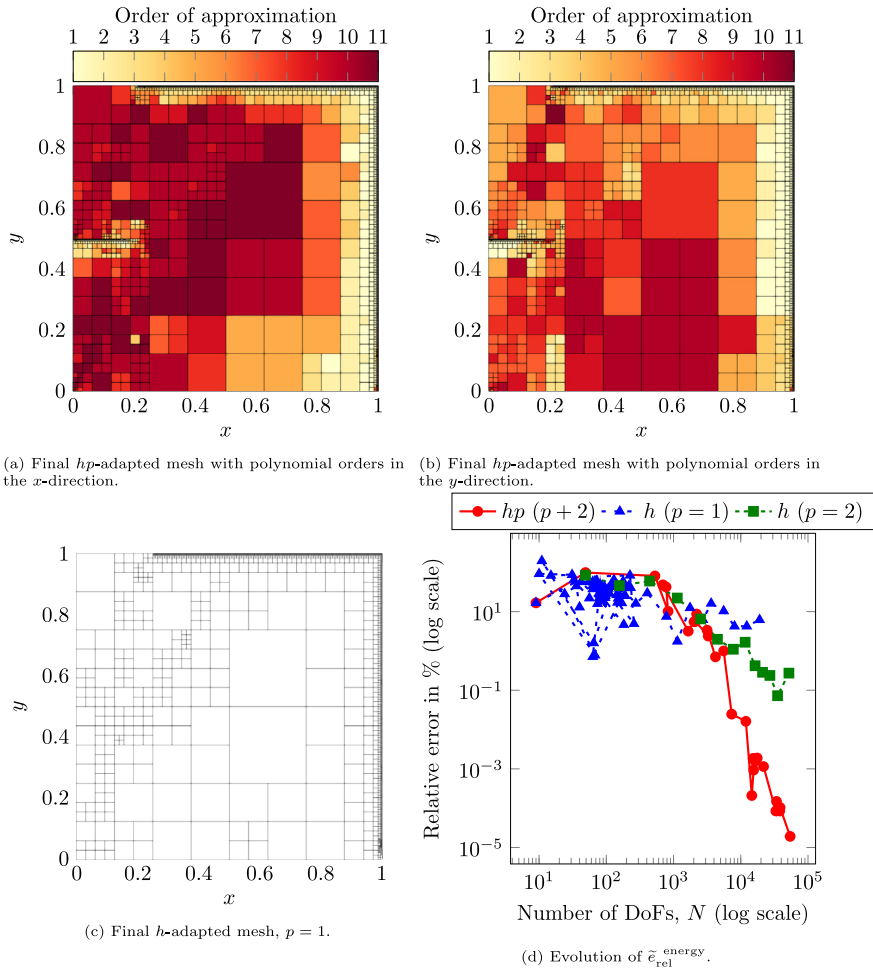


Fig. 16. Final h - and hp -adapted meshes for our convection-dominated diffusion example 2 and the evolution of \tilde{e}_{rel}^{energy} .

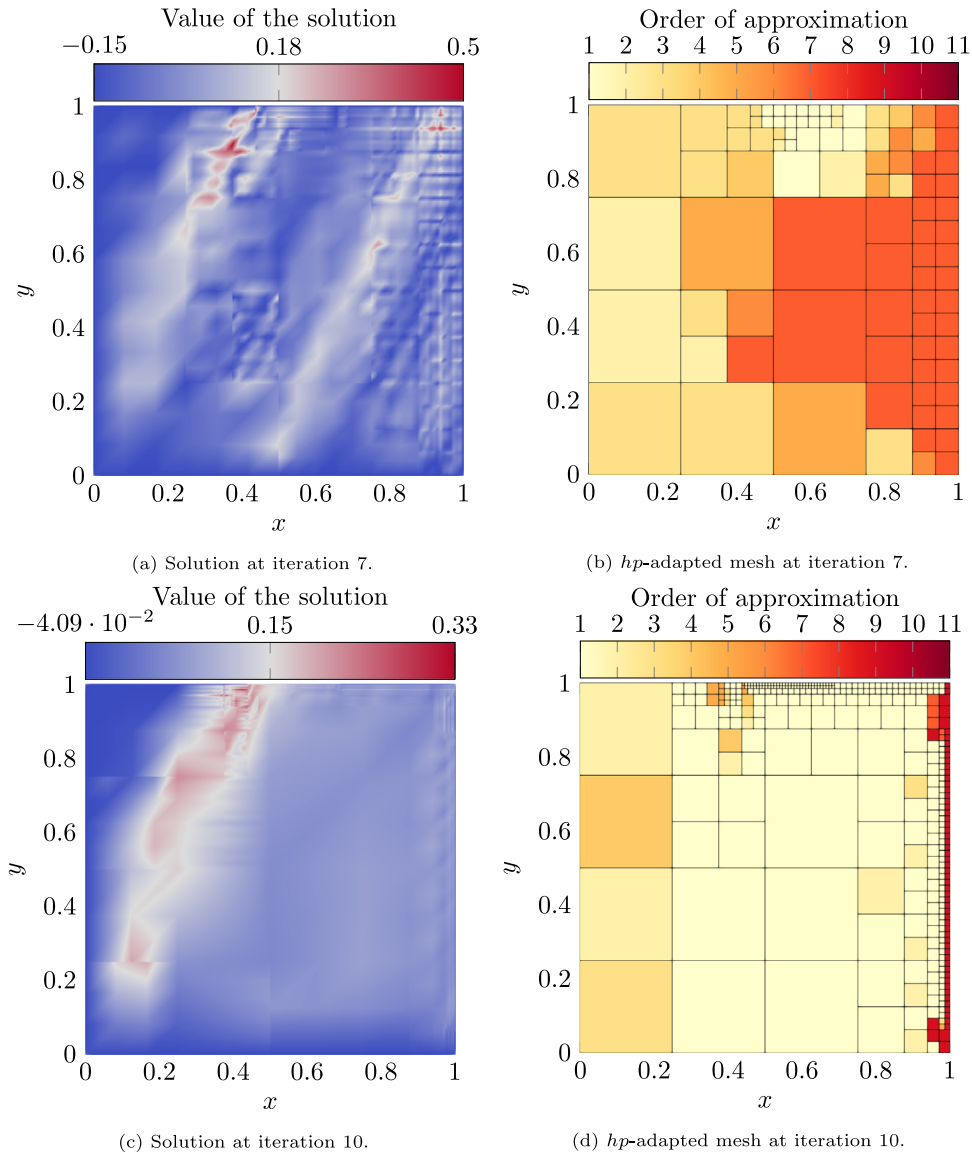


Fig. 17. Numerical solutions and hp -adapted meshes (polynomial orders in the x -direction) at iterations 7 and 10.

We also highlight the gradual behavior of the adaptive process: at the beginning, the refinements are mostly introduced to capture the boundary layers (Fig. 17d). Once the boundary layers are properly resolved (Fig. 18b), the algorithm refines to catch better the direction of propagation of the convection part of the problem. The adaptive process is almost finished at this point, and the error is of the order of $10^{-4}\%$. The final refinements are devoted to improving the solution nearby the source discontinuity, and accordingly, we begin to observe more refinements towards this region (see Fig. 18d). The final meshes (iteration 27) correspond to Figs. 16a and 16b.

4.4.2. Goal-oriented adaptivity

We select the domain of the QoI (illustrated in Fig. 14(a)) to be $\Omega_I = (\frac{3}{4}, 1)^2 \subset \Omega$. Fig. 19 displays the solutions to the forward and adjoint problems associated with the second example. As expected, we observe (a) higher resolution at the QoI –upper-right part of the domain–, and (b) spurious numerical oscillations in the forward problem far from the region of interest where the QoI is defined (compared to the energy-norm solution depicted in Fig. 15).

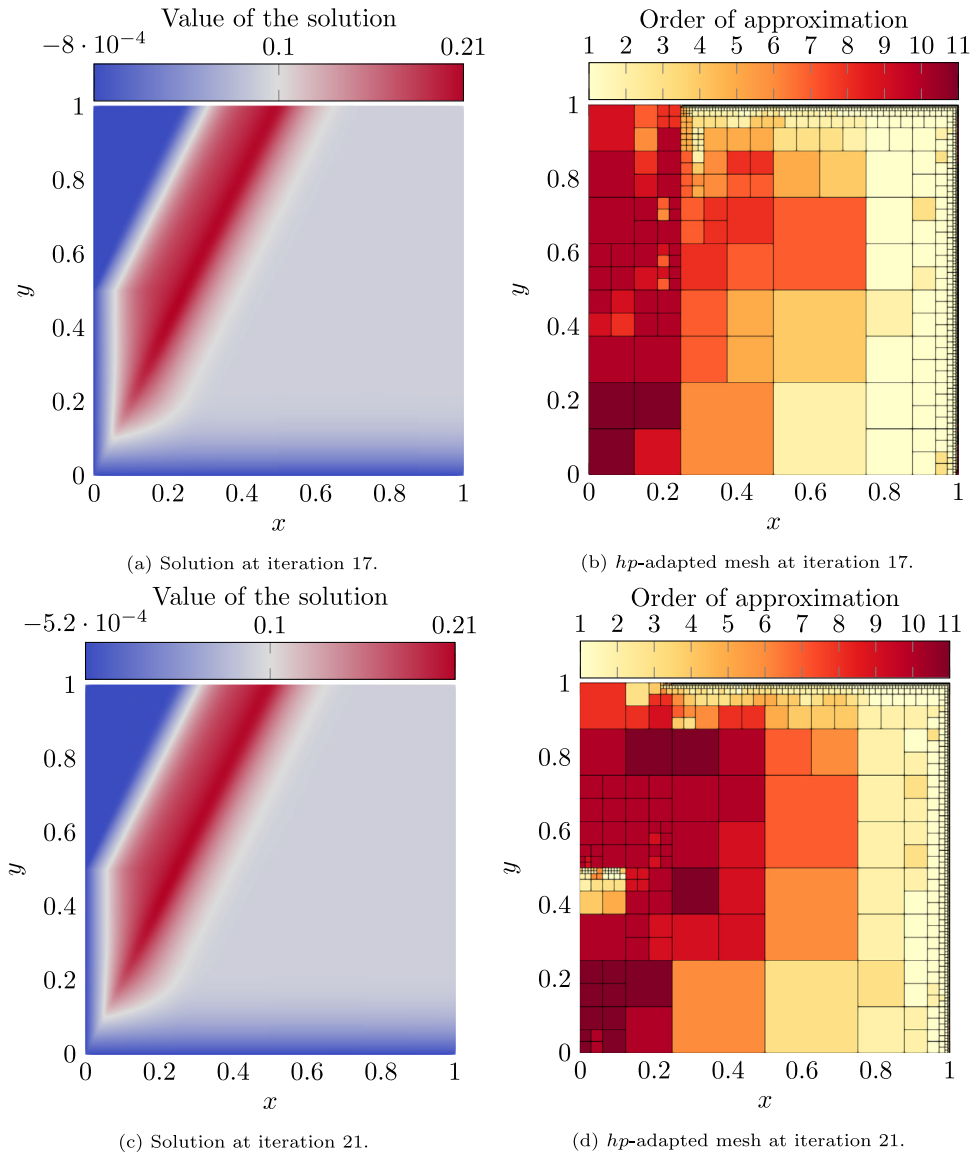


Fig. 18. Numerical solutions and hp -adapted meshes (polynomial orders in the x -direction) at iterations 17 and 21.

Fig. 20 displays the final h - and hp -adapted meshes and the evolution of $e_{\text{rel}}^{\text{Qol}}$. In contrast to the energy-norm adaptivity, where the refinements were more oriented towards the top and right boundary, here, the adjoint problem (Fig. 19b) highly drives the refinements for both h - and hp -strategies, and hence, we observe further refinements on the boundary layers of the adjoint problem.

4.5. 3D numerical results

Let us consider the following non-elliptic problem based on heterogeneous Helmholtz's equation.

$$\left| \begin{array}{l} \text{Find } u \text{ such that,} \\ -\nabla \cdot (\sigma \nabla u) - k^2 u = \mathbb{1}_{\Omega_f} \text{ in } \Omega, \\ u = 0 \quad \text{on } \Gamma_D, \end{array} \right. \quad (46)$$

$$u = 0 \quad \text{on } \Gamma_D, \quad (47)$$

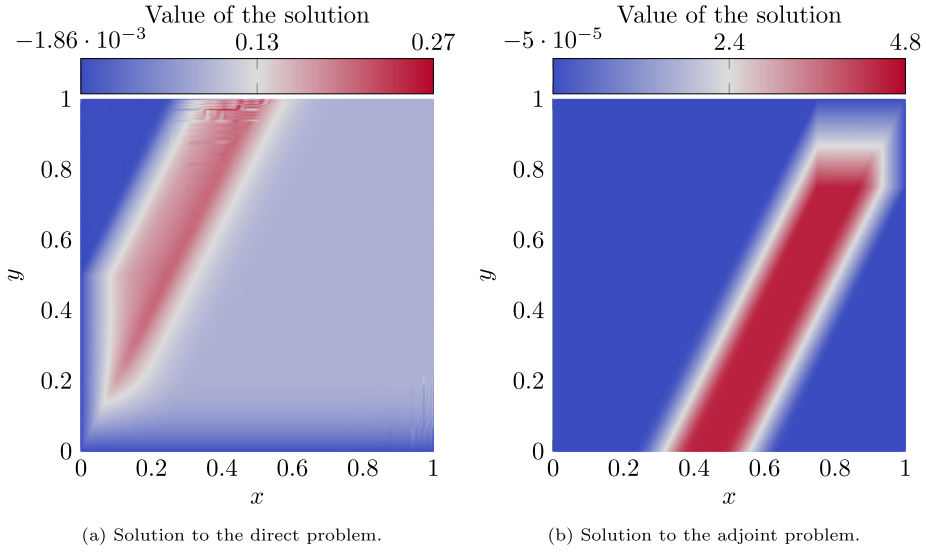


Fig. 19. Direct and adjoint numerical solutions of the convection-dominated diffusion problem for GOA.

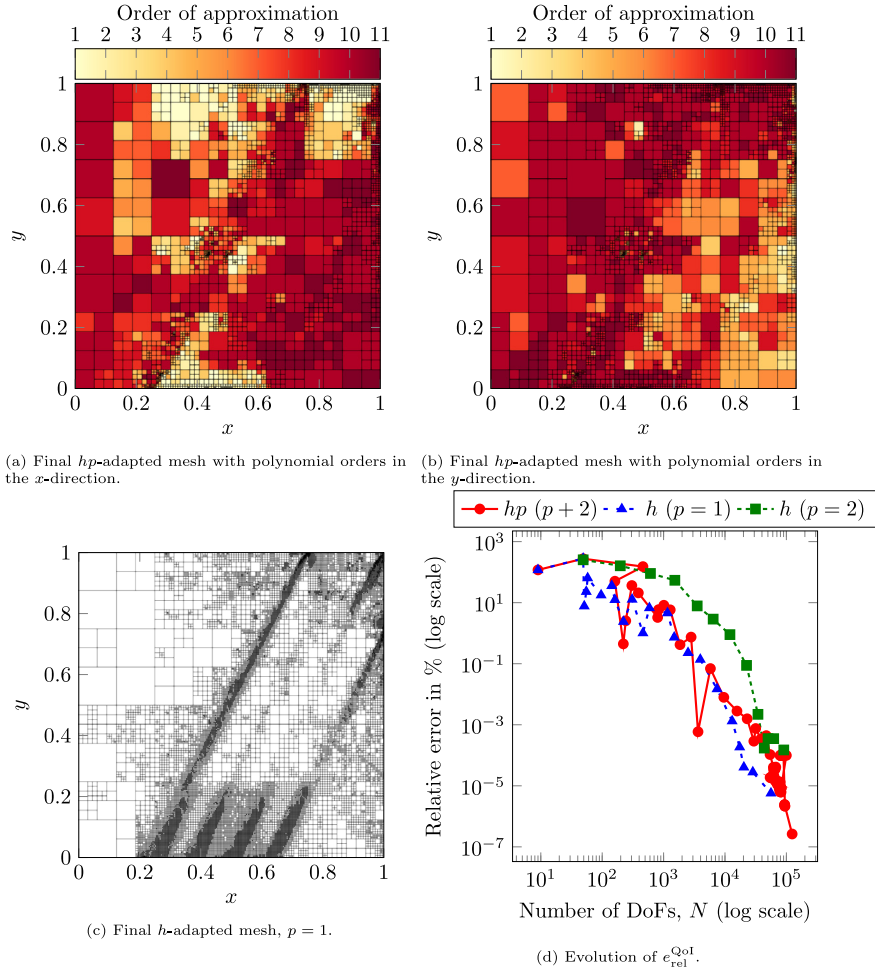


Fig. 20. Final h - and hp -adapted meshes for our convection-dominated diffusion second example and the evolution of $e_{\text{rel}}^{\text{Qol}}$.

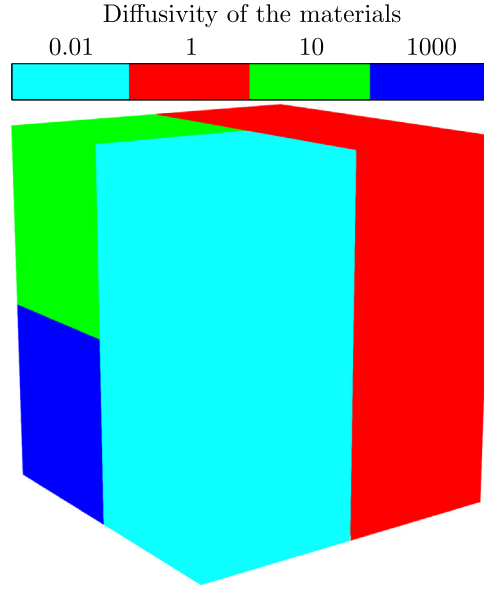


Fig. 21. Diffusive coefficient values for the different materials in the domain.

$$\nabla u \cdot \vec{n} = 0 \quad \text{on } \Gamma_N, \quad (48)$$

where $\Omega = (0, 1)^3 \subset \mathbb{R}^3$, $\Omega_f = (0, \frac{1}{4})^3 \subset \Omega$, and $k = (4 \cdot 2\pi, 2\pi)$. Γ_D and Γ_N stand for the parts of the boundary $\partial\Omega$ where we impose homogeneous Dirichlet and Neumann boundary conditions, respectively. We impose Dirichlet boundary conditions on the 3 faces whose intersection is $(0, 0, 0)$ and Neumann boundary on the 3 faces whose intersection is $(1, 1, 1)$.

$$\Gamma_D := ([0, 1] \times [0, 1] \times \{0\}) \cup ([0, 1] \times \{0\} \times [0, 1]) \cup (\{0\} \times [0, 1] \times [0, 1]), \quad (49)$$

$$\Gamma_N := ((0, 1) \times (0, 1) \times \{1\}) \cup ((0, 1) \times \{1\} \times (0, 1)) \cup (\{1\} \times (0, 1) \times (0, 1)). \quad (50)$$

Here,

$$\sigma(x) = \begin{cases} 1 & \text{if } x \in \Omega_1 = \{0 < x < 1, 0 < y < \frac{1}{2}, 0 < z < 1\}, \\ 10^3 & \text{if } x \in \Omega_2 = \{\frac{1}{2} < x < 1, \frac{1}{2} < y < 1, 0 < z < \frac{1}{2}\}, \\ 10 & \text{if } x \in \Omega_3 = \{\frac{1}{2} < x < 1, \frac{1}{2} < y < 1, \frac{1}{2} < z < 1\}, \\ 10^{-2} & \text{if } x \in \Omega_4 = \{0 < x < \frac{1}{2}, \frac{1}{2} < y < 1, 0 < z < 1\}. \end{cases}$$

We define the operators $b(\cdot, \cdot)$ and $a(\cdot, \cdot)$ associated with the above problem as follows:

$$b(\cdot, \cdot) := \langle \nabla \cdot, \sigma \nabla \cdot \rangle_{L^2(\Omega)} - k^2 \langle \cdot, \cdot \rangle_{L^2(\Omega)}, \quad a(\cdot, \cdot) := |\langle \nabla \cdot, \sigma \nabla \cdot \rangle_{L^2(\Omega)}| + |k^2| |\langle \cdot, \cdot \rangle_{L^2(\Omega)}|. \quad (51)$$

Once again, $\|\cdot\|_e^2 = a(\cdot, \cdot)$ is our energy norm and $|b(\phi, \psi)| \leq |a(\phi, \psi)|$, $\forall \phi, \psi \in \mathbb{H}$.

Fig. 21 displays the different materials in the domain. Following the definition of Eq. (34), we select $\Omega_l = (\frac{3}{4}, 1)^3 \subset \Omega$. For goal-oriented adaptivity, Figs. 22a and 22b show the solutions of the direct and adjoint problems, respectively.

Figs. 23 and 24 display the final hp -adapted meshes for our 3D wave propagation example in a lossy medium using energy-norm and goal-oriented adaptivity, respectively. The initial uniform mesh is composed of sixty-four root elements. As expected, we observe heavy h -refinements near different materials' interfaces. Fig. 25 shows the corresponding convergence curves. As in the 2D case, the energy-norm hp -adaptivity provides proper convergence results in terms of energy. However, the convergence of the energy-norm adaptivity in terms of the error in the QoI is slow, especially in the pre-asymptotic regime. When using goal-oriented adaptivity, the evolution of the error in the QoI exhibits much better behavior, while the energy convergence becomes suboptimal, as expected.

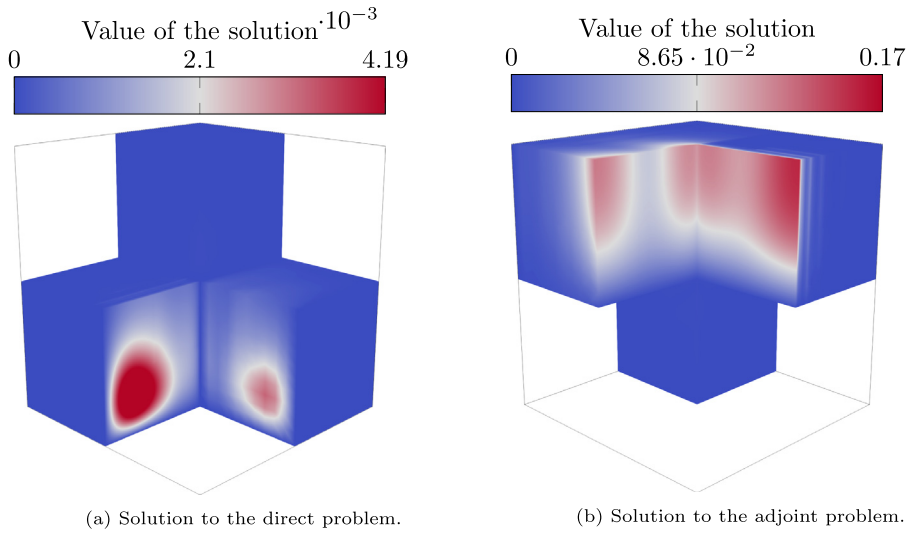


Fig. 22. Absolute value of the direct and adjoint solutions of our 3D wave propagation example in a lossy medium.

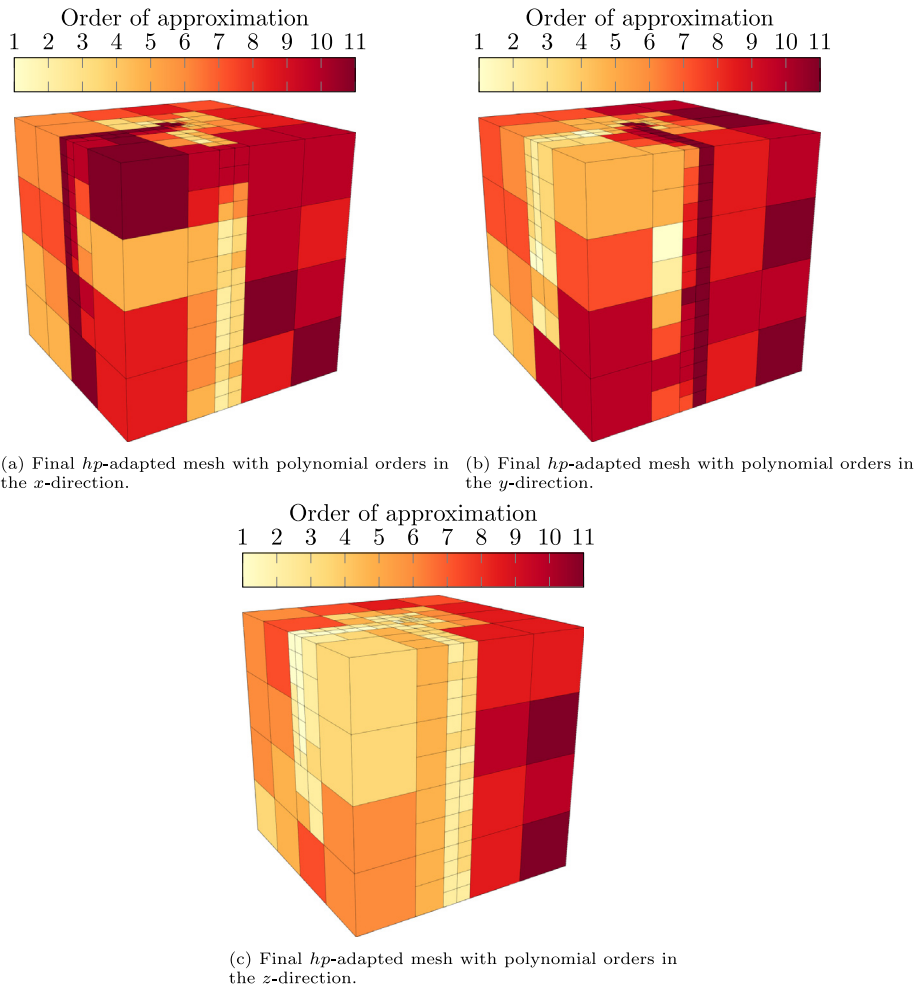


Fig. 23. Energy-norm adaptivity. Final hp -adapted meshes for our 3D wave propagation example in a lossy medium.

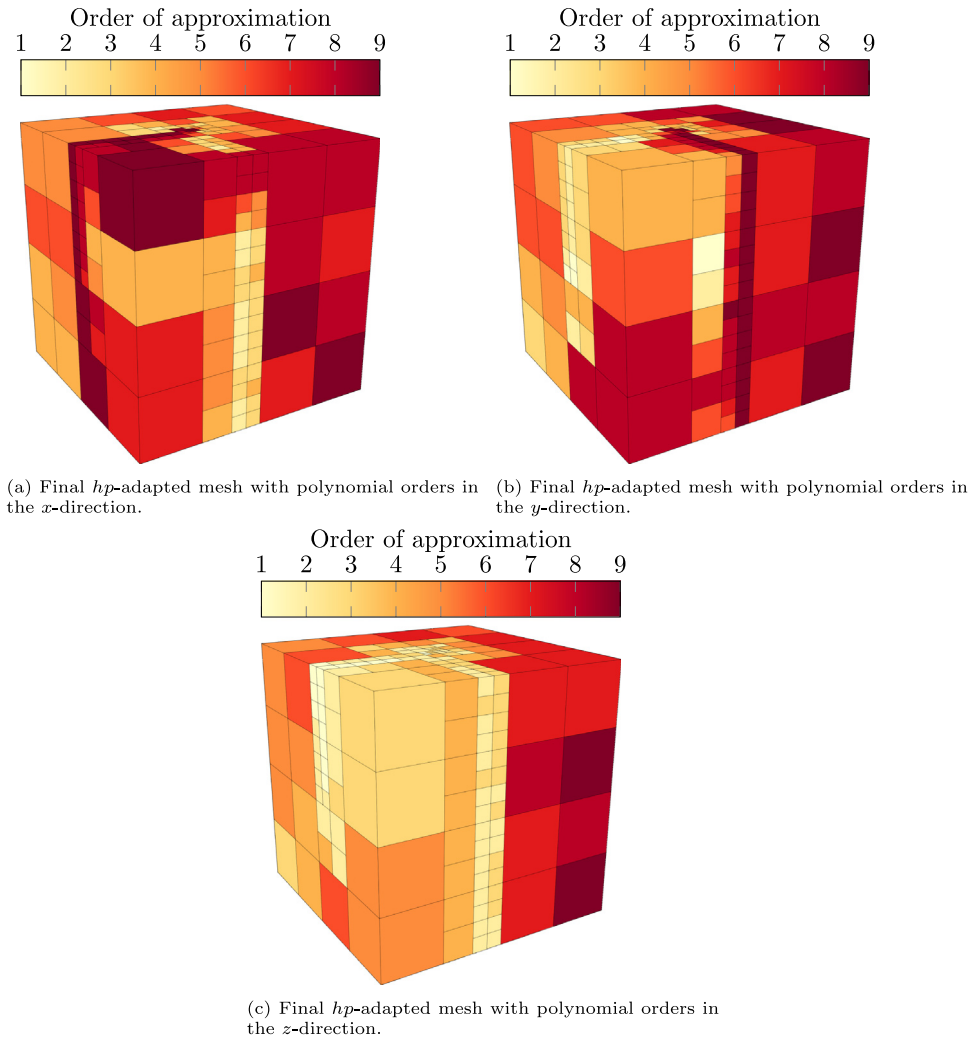


Fig. 24. Goal-oriented adaptivity. Final hp -adapted meshes for our 3D wave propagation example in a lossy medium.

5. Conclusions

This work employs an automatically adaptive mesh-generation strategy that alternates refinement steps with quasi-optimal hp -unrefinement actions. The basis functions with the lowest contribution to the solution are removed during the coarsening part.

How to efficiently identify which basis functions to remove is challenging. In this regard, in this work, we extend an existing coarsening strategy suitable for energy-norm adaptivity to non-elliptic problems and goal-oriented adaptive strategies. In particular, we estimate the contribution of the basis functions to the solution in terms of an inner product associated with the bilinear form of the problem, and then, each coarsening step removes the basis functions according to these new estimations. The resulting algorithm is easy-to-implement since it employs hierarchical data structures that avoid the need for the so-called 1-irregularity rule for handling *hanging nodes*.

Our numerical results show the performance of our algorithm by solving different 2D and 3D problems based on Poisson, Helmholtz, and convection-dominated equations, and they demonstrate the robustness and fast convergence of our hp -adaptive method. Thus, these results and the straightforward implementation of our approach suggest that this approach can be easily adapted to industrial applications.

Possible extensions of this work include anisotropic h -refinements and electromagnetic applications. For the latter purpose, the hierarchical data structures require an extension to $H(\text{curl})$ conforming to finite element spaces.

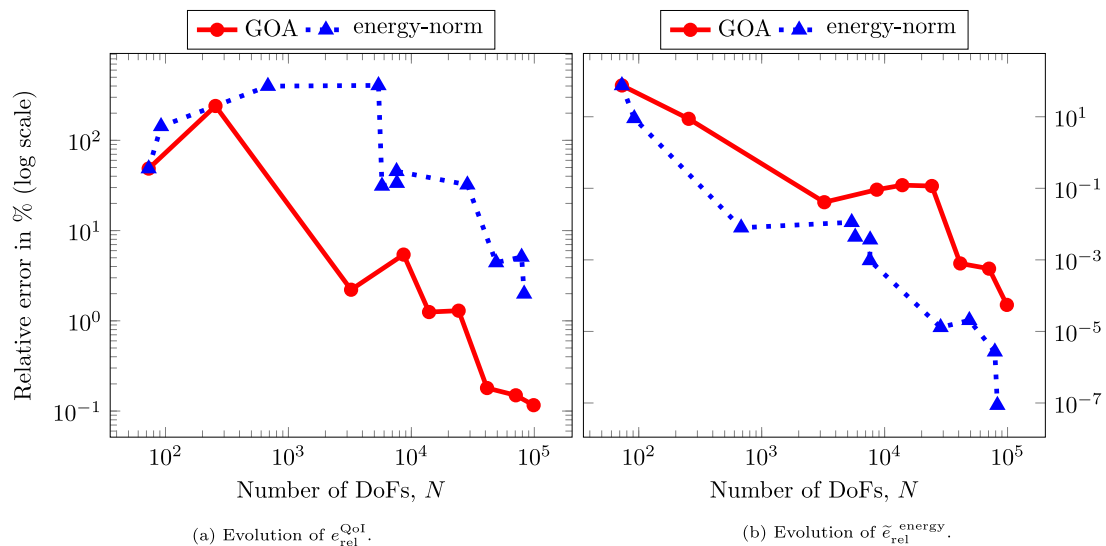


Fig. 25. Convergence history of $e_{\text{rel}}^{\text{QoI}}$ and $\tilde{e}_{\text{rel}}^{\text{energy}}$ for the energy-norm and GOA hp -adaptive strategies.

Declaration of competing interest

The authors declare that they have no known competing financial interests or personal relationships that could have appeared to influence the work reported in this paper.

Data availability

No data was used for the research described in the article.

References

- [1] S. Larsson, V. Thomée, Partial Differential Equations with Numerical Methods, Vol. 45, Springer Science & Business Media, 2008, <http://dx.doi.org/10.1007/978-3-540-88706-5>.
- [2] C. Johnson, Numerical Solution of Partial Differential Equations By the Finite Element Method, Courier Corporation, 2012.
- [3] T. Belytschko, M. Tabbara, H-adaptive finite element methods for dynamic problems, with emphasis on localization, Internat. J. Numer. Methods Engrg. 36 (24) (1993) 4245–4265, <http://dx.doi.org/10.1002/nme.1620362409>.
- [4] I. Babuška, B.A. Szabo, I.N. Katz, The p-version of the finite element method, SIAM J. Numer. Anal. 18 (3) (1981) 515–545, <http://dx.doi.org/10.1137/0718033>.
- [5] I. Babuška, M.R. Dorr, Error estimates for the combined h and p versions of the finite element method, Numer. Math. 37 (2) (1981) 257–277, <http://dx.doi.org/10.1007/BF01398256>.
- [6] J.T. Oden, A. Patra, A parallel adaptive strategy for hp finite element computations, Comput. Methods Appl. Mech. Engrg. 121 (1–4) (1995) 449–470, [http://dx.doi.org/10.1016/0045-7825\(94\)00705-R](http://dx.doi.org/10.1016/0045-7825(94)00705-R), URL <https://www.sciencedirect.com/science/article/pii/004578259400705R>.
- [7] L. Demkowicz, W. Rachowicz, P. Devloo, A fully automatic hp -adaptivity, J. Sci. Comput. 17 (1) (2002) 117–142, <http://dx.doi.org/10.1023/A:1015192312705>.
- [8] L. Demkowicz, Computing with hp -Adaptive Finite Elements. Vol. 1. One and Two Dimensional Elliptic and Maxwell Problems, in: Applied Mathematics and Nonlinear Science Series, Chapman & Hall/CRC, Boca Raton, FL, 2007, p. xxvi+398, <http://dx.doi.org/10.1201/9781420011692>.
- [9] L. Demkowicz, J. Kurtz, D. Pardo, M. Paszyński, W. Rachowicz, A. Zdunek, Computing with hp -adaptive finite elements. Vol. 2. Frontiers: three dimensional elliptic and maxwell problems with applications, in: Applied Mathematics and Nonlinear Science Series, Chapman & Hall/CRC, Boca Raton, FL, 2008, p. xvi+417, <http://dx.doi.org/10.1201/9781420011692>.
- [10] M. Paszyński, L. Demkowicz, D. Pardo, Verification of goal-oriented hp -adaptivity, Comput. Math. Appl. 50 (8–9) (2005) 1395–1404, <http://dx.doi.org/10.1016/j.camwa.2005.03.018>, URL <https://www.sciencedirect.com/science/article/pii/S0898122105003895>.
- [11] L.E. Garcia-Castillo, D. Pardo, I. Gomez-Revuelto, L.F. Demkowicz, A two-dimensional self-adaptive hp finite element method for the characterization of waveguide discontinuities. Part I: Energy-norm based automatic hp -adaptivity, Comput. Methods Appl. Mech. Engrg. 196 (49–52) (2007) 4823–4852, <http://dx.doi.org/10.1016/j.cma.2007.06.024>, URL <https://www.sciencedirect.com/science/article/pii/S0045782507002939>.

- [12] D. Pardo, L.E. García-Castillo, L.F. Demkowicz, C. Torres-Verdín, A two-dimensional self-adaptive *hp* finite element method for the characterization of waveguide discontinuities. Part II: Goal-oriented *hp*-adaptivity, *Comput. Methods Appl. Mech. Engrg.* 196 (49–52) (2007) 4811–4822, <http://dx.doi.org/10.1016/j.cma.2007.06.023>, URL <https://www.sciencedirect.com/science/article/pii/S0045782507002940>.
- [13] D. Pardo, L. Demkowicz, C. Torres-Verdín, C. Michler, PML enhanced with a self-adaptive goal-oriented *hp*-finite element method: Simulation of through-casing borehole resistivity measurements, *SIAM J. Sci. Comput.* 30 (6) (2008) 2948–2964, <http://dx.doi.org/10.1137/070689796>.
- [14] I. Gomez-Revuelto, L.E. Garcia-Castillo, S. Llorente-Romano, D. Pardo, A three-dimensional self-adaptive *hp* finite element method for the characterization of waveguide discontinuities, *Comput. Methods Appl. Mech. Engrg.* 249 (2012) 62–74, <http://dx.doi.org/10.1016/j.cma.2012.05.013>, URL <https://www.sciencedirect.com/science/article/pii/S0045782512001624>.
- [15] M. Paszyński, D. Pardo, V. Calo, Parallel simulations of 3D DC borehole resistivity measurements with goal-oriented self-adaptive *hp* finite element method, *J. Serbian Soc. Comput. Mech.* 6 (2) (2012) 1–18.
- [16] J. Alvarez-Aramberri, *hp-Adaptive Simulation and Inversion of Magnetotelluric Measurements* (Ph.D. thesis), Universidad del País Vasco-Euskal Herriko Unibertsitatea. Pau (INRIA), 2015.
- [17] M. Ainsworth, B. Senior, An adaptive refinement strategy for *hp*-finite element computations, *Appl. Numer. Math.* 26 (1–2) (1998) 165–178, [http://dx.doi.org/10.1016/S0168-9274\(97\)00083-4](http://dx.doi.org/10.1016/S0168-9274(97)00083-4), URL <https://www.sciencedirect.com/science/article/pii/S0168927497000834>.
- [18] P. Houston, C. Schwab, E. Süli, Discontinuous *hp*-finite element methods for advection-diffusion-reaction problems, *SIAM J. Numer. Anal.* 39 (6) (2002) 2133–2163, <http://dx.doi.org/10.1137/S0036142900374111>.
- [19] P.F. Antonietti, S. Giani, P. Houston, *hp*-Version composite discontinuous Galerkin methods for elliptic problems on complicated domains, *SIAM J. Sci. Comput.* 35 (3) (2013) A1417–A1439, <http://dx.doi.org/10.1137/120877246>.
- [20] W.F. Mitchell, M.A. McClain, A comparison of *hp*-adaptive strategies for elliptic partial differential equations, *ACM Trans. Math. Software* 41 (1) (2014) 2:1–2:39, <http://dx.doi.org/10.1145/2629459>, URL <http://doi.acm.org/10.1145/2629459>.
- [21] P. Solin, K. Segeth, I. Dolezel, *Higher-Order Finite Element Methods*, Chapman and Hall/CRC, 2003, <http://dx.doi.org/10.1201/9780203488041>.
- [22] N. Zander, T. Bog, S. Kollmannsberger, D. Schillinger, E. Rank, Multi-level *hp*-adaptivity: high-order mesh adaptivity without the difficulties of constraining hanging nodes, *Comput. Mech.* 55 (3) (2015) 499–517, <http://dx.doi.org/10.1007/s00466-014-1118-x>.
- [23] P. Kopp, E. Rank, V.M. Calo, S. Kollmannsberger, Efficient multi-level *hp*-finite elements in arbitrary dimensions, *Comput. Methods Appl. Mech. Engrg.* 401 (3) (2022) 499–517, <http://dx.doi.org/10.1016/j.cma.2022.115575>, URL <https://www.sciencedirect.com/science/article/pii/S0045782522005515>.
- [24] P. Kopp, V. Calo, E. Rank, S. Kollmannsberger, Space-time *hp*-finite elements for heat evolution in laser powder bed fusion additive manufacturing, *Engineering with Computers* (2022) <http://dx.doi.org/10.1007/s00366-022-01719-1>, URL <https://doi.org/10.1007/s00366-022-01719-1>.
- [25] V. Darrigrand, D. Pardo, T. Chaumont-Frelet, I. Gómez-Revuelto, L.E. Garcia-Castillo, A painless automatic *hp*-adaptive strategy for elliptic problems, *Finite Elem. Anal. Des.* 178 (2020) 103424, <http://dx.doi.org/10.1016/j.finel.2020.103424>, URL <https://www.sciencedirect.com/science/article/pii/S0168874X20301049>.
- [26] N. Zander, T. Bog, M. Elhaddad, F. Frischmann, S. Kollmannsberger, E. Rank, The multi-level *hp*-method for three-dimensional problems: Dynamically changing high-order mesh refinement with arbitrary hanging nodes, *Comput. Methods Appl. Mech. Engrg.* 310 (2016) 252–277, <http://dx.doi.org/10.1016/j.cma.2016.07.007>, URL <http://www.sciencedirect.com/science/article/pii/S0045782516307289>.
- [27] N.D. Zander, *Multi-Level *hp*-FEM: Dynamically Changing High-Order Mesh Refinement with Arbitrary Hanging Nodes* (Ph.D. thesis), Technische Universit.
- [28] P. Binev, Instance optimality for *hp*-type approximation, *Oberwolfach Rep.* 39 (2013) 14–16, <http://dx.doi.org/10.4171/OWR/2013/39>.
- [29] C. Canuto, R.H. Nochetto, R. Stevenson, M. Verani, Convergence and optimality of *hp*-AFEM, *Numer. Math.* 135 (4) (2017) 1073–1119, <http://dx.doi.org/10.1007/s00211-016-0826-x>, 3621826.
- [30] M. Ainsworth, J.T. Oden, A posteriori error estimation in finite element analysis, *Comput. Methods Appl. Mech. Engrg.* 142 (1–2) (1997) 1–88, [http://dx.doi.org/10.1016/S0045-7825\(96\)01107-3](http://dx.doi.org/10.1016/S0045-7825(96)01107-3), URL <https://www.sciencedirect.com/science/article/pii/S0045782596011073>.
- [31] R. Becker, R. Rannacher, *Weighted a Posteriori Error Control in FE Methods* (Ph.D. thesis), IWR, 1996.
- [32] R. Rannacher, F.-T. Suttmeier, A posteriori error control in finite element methods via duality techniques: application to perfect plasticity, *Comput. Mech.* 21 (2) (1998) 123–133, <http://dx.doi.org/10.1007/s004660050288>.
- [33] S. Prudhomme, J.T. Oden, On goal-oriented error estimation for elliptic problems: application to the control of pointwise errors, *Comput. Methods Appl. Mech. Engrg.* 176 (1–4) (1999) 313–331, [http://dx.doi.org/10.1016/S0045-7825\(98\)00343-0](http://dx.doi.org/10.1016/S0045-7825(98)00343-0).
- [34] J.T. Oden, S. Prudhomme, Goal-oriented error estimation and adaptivity for the finite element method, *Comput. Math. Appl.* 41 (5–6) (2001) 735–756, [http://dx.doi.org/10.1016/S0898-1221\(00\)00317-5](http://dx.doi.org/10.1016/S0898-1221(00)00317-5).
- [35] D. Pardo, L. Demkowicz, C. Torres-Verdín, L. Tabarovsky, A goal-oriented *hp*-adaptive finite element method with electromagnetic applications. i. electrostatics, *Internat. J. Numer. Methods Engrg.* 65 (8) (2006) 1269–1309, <http://dx.doi.org/10.1002/nme.1488>.
- [36] D. Pardo, L. Demkowicz, C. Torres-Verdín, M. Paszynski, A self-adaptive goal-oriented *hp* finite element method with electromagnetic applications. II. Electrodynamics, *Comput. Methods Appl. Mech. Engrg.* 196 (37–40) (2007) 3585–3597, <http://dx.doi.org/10.1016/j.cma.2006.10.016>.
- [37] D. Pardo, Multigoal-oriented adaptivity for *hp*-finite element methods, *Procedia Comput. Sci.* 1 (1) (2010) 1953–1961, <http://dx.doi.org/10.1016/j.procs.2010.04.219>, URL <http://www.sciencedirect.com/science/article/pii/S1877050910002206>.
- [38] J. Alvarez-Aramberri, D. Pardo, Dimensionally adaptive *hp*-finite element simulation and inversion of 2D magnetotelluric measurements, *J. Comput. Sci.* 18 (2017) 95–105, <http://dx.doi.org/10.1016/j.jocs.2016.07.014>, URL <https://www.sciencedirect.com/science/article/pii/S1877750316301223>.

- [39] J. Panetier, P. Ladevèze, L. Chamoin, Strict and effective bounds in goal-oriented error estimation applied to fracture mechanics problems solved with XFEM, *Internat. J. Numer. Methods Engrg.* 81 (6) (2010) 671–700, <http://dx.doi.org/10.1002/nme.2705>.
- [40] J. Waeytens, L. Chamoin, P. Ladevèze, Guaranteed error bounds on pointwise quantities of interest for transient viscodynamics problems, *Comput. Mech.* 49 (3) (2012) 291–307, <http://dx.doi.org/10.1007/s00466-011-0642-1>, 2891605.
- [41] F. Verdugo, P. Díez, Computable bounds of functional outputs in linear visco-elastodynamics, *Comput. Methods Appl. Mech. Engrg.* 245/246 (2012) 313–330, <http://dx.doi.org/10.1016/j.cma.2012.06.016>, 2981893.
- [42] K.G. Van der Zee, E.H. Van Brummelen, I. Akkerman, R. de Borst, Goal-oriented error estimation and adaptivity for fluid-structure interaction using exact linearized adjoints, *Comput. Methods Appl. Mech. Engrg.* 200 (37–40) (2011) 2738–2757, <http://dx.doi.org/10.1016/j.cma.2010.12.010>.
- [43] K.G. Van Der Zee, J. Tinsley Oden, S. Prudhomme, A. Hawkins-Daarud, Goal-oriented error estimation for Cahn–Hilliard models of binary phase transition, *Numer. Methods Partial Differential Equations* 27 (1) (2011) 160–196, <http://dx.doi.org/10.1002/num.20638>.
- [44] K.G. Van der Zee, C.V. Verhoosel, Isogeometric analysis-based goal-oriented error estimation for free-boundary problems, *Finite Elem. Anal. Des.* 47 (6) (2011) 600–609, <http://dx.doi.org/10.1016/j.finel.2010.12.013>.
- [45] T. Wick, Goal-oriented mesh adaptivity for fluid-structure interaction with application to heart-valve settings, *Arch. Mech. Eng.* 59 (1) (2012) 73–99.
- [46] M. Hintermüller, R.H. Hoppe, Goal-oriented adaptivity in pointwise state constrained optimal control of partial differential equations, *SIAM J. Control Optim.* 48 (8) (2010) 5468–5487, <http://dx.doi.org/10.1137/090761823>.
- [47] A. Günther, M. Hinze, M.H. Tber, A posteriori error representations for elliptic optimal control problems with control and state constraints, in: *Constrained Optimization and Optimal Control for Partial Differential Equations*, Springer Basel, Basel, 2012, pp. 303–317, http://dx.doi.org/10.1007/978-3-0348-0133-1_17.
- [48] M. Hintermüller, R. Hoppe, C. Löbhard, Dual-weighted goal-oriented adaptive finite elements for optimal control of elliptic variational inequalities, *ESAIM Control Optim. Calc. Var.* 20 (2014) 524–546, <http://dx.doi.org/10.1051/cocv/2013074>.
- [49] V. Darrigrand, D. Pardo, I. Muga, Goal-oriented adaptivity using unconventional error representations for the 1D Helmholtz equation, *Comput. Math. Appl.* 69 (9) (2015) 964–979, <http://dx.doi.org/10.1016/j.camwa.2015.03.006>, URL <http://www.sciencedirect.com/science/article/pii/S0898122115001017>.
- [50] M. Holst, S. Pollock, Y. Zhu, Convergence of goal-oriented adaptive finite element methods for semilinear problems, *Comput. Vis. Sci.* 17 (1) (2015) 43–63, <http://dx.doi.org/10.1007/s00791-015-0243-1>.
- [51] V. Darrigrand, Á. Rodríguez-Rozas, I. Muga, D. Pardo, A. Romkes, S. Prudhomme, Goal-oriented adaptivity using unconventional error representations for the multi-dimensional Helmholtz equation, *Internat. J. Numer. Methods Engrg.* 113 (1) (2018) 22–42, <http://dx.doi.org/10.1002/nme.5601>, nme.5601.
- [52] M. Holst, S. Pollock, Convergence of goal-oriented adaptive finite element methods for nonsymmetric problems, *Numer. Methods Partial Differential Equations* 32 (2) (2016) 479–509, <http://dx.doi.org/10.1002/num.22002>.
- [53] E. Valseth, A. Romkes, Goal-oriented error estimation for the automatic variationally stable FE method for convection-dominated diffusion problems, *Comput. Math. Appl.* 80 (12) (2020) 3027–3043, <http://dx.doi.org/10.1016/j.camwa.2020.10.019>, URL <https://www.sciencedirect.com/science/article/pii/S0898122120304211>.
- [54] W. Rachowicz, D. Pardo, L. Demkowicz, Fully automatic hp -adaptivity in three dimensions, *Comput. Methods Appl. Mech. Engrg.* 195 (37–40) (2006) 4816–4842, <http://dx.doi.org/10.1016/j.cma.2005.08.022>.
- [55] N. Zander, H. Bériot, C. Hoff, P. Kodl, L. Demkowicz, Anisotropic multi-level hp -refinement for quadrilateral and triangular meshes, *Finite Elem. Anal. Des.* 203 (2022) 103700, <http://dx.doi.org/10.1016/j.finel.2021.103700>, URL <https://www.sciencedirect.com/science/article/pii/S0168874X21001748>.
- [56] W. Rachowicz, L. Demkowicz, An hp -adaptive finite element method for electromagnetics: Part 1: Data structure and constrained approximation, *Comput. Methods Appl. Mech. Engrg.* 187 (1–2) (2000) 307–335, [http://dx.doi.org/10.1016/S0045-7825\(99\)00137-1](http://dx.doi.org/10.1016/S0045-7825(99)00137-1), URL <https://www.sciencedirect.com/science/article/pii/S0045782599001371>.
- [57] C. Mote Jr., Global-local finite element, *Internat. J. Numer. Methods Engrg.* 3 (4) (1971) 565–574, <http://dx.doi.org/10.1002/nme.1620030410>, URL <https://onlinelibrary.wiley.com/doi/abs/10.1002/nme.1620030410>.
- [58] S. Franz, T. Linß, Superconvergence analysis of the Galerkin FEM for a singularly perturbed convection–diffusion problem with characteristic layers, *Numer. Methods Partial Differ. Equ. Int. J.* 24 (1) (2008) 144–164, <http://dx.doi.org/10.1002/num.20245>, URL <https://onlinelibrary.wiley.com/doi/abs/10.1002/num.20245>.
- [59] S. Franz, G. Matthies, Local projection stabilisation on S-type meshes for convection–diffusion problems with characteristic layers, *Computing* 87 (3) (2010) 135–167, <http://dx.doi.org/10.1007/s00607-010-0079-y>.
- [60] S. Franz, H.-G. Roos, Error estimation in a balanced norm for a convection–diffusion problem with two different boundary layers, *Calcolo* 51 (3) (2014) 423–440, <http://dx.doi.org/10.1007/s10092-013-0093-5>.
- [61] M. Stynes, L. Tobiska, The SDFEM for a convection–diffusion problem with a boundary layer: Optimal error analysis and enhancement of accuracy, *SIAM J. Numer. Anal.* 41 (5) (2003) 1620–1642, <http://dx.doi.org/10.1137/S0036142902404728>.
- [62] R. Verfürth, Robust a posteriori error estimates for stationary convection–diffusion equations, *SIAM J. Numer. Anal.* 43 (4) (2005) 1766–1782, <http://dx.doi.org/10.1137/040604261>.
- [63] J.A. Cottrell, T.J. Hughes, Y. Bazilevs, *Isogeometric Analysis: Toward Integration of CAD and FEA* (Ph.D. thesis), John Wiley & Sons, 2009.